Higgs-mode-induced instability and kinetic inductance in strongly dc-biased dirty-limit superconductors

Takayuki Kubo[*]

High Energy Accelerator Research Organization (KEK), Tsukuba, Ibaraki 305-0801, Japan and
The Graduate University for Advanced Studies (Sokendai), Hayama, Kanagawa 240-0193, Japan

A perturbative ac field superposed on a dc bias (J_b) is known to excite the Higgs mode in superconductors. The dirty limit, where disorder enhances the Higgs resonance, provides an ideal setting for this study and is also relevant to many superconducting devices operating under strong dc biases. However, the effects of a strong dc bias near the depairing current in dirty-limit superconductors remain largely unexplored, despite their significance in both fundamental physics and applications. In this paper, we derive a general formula for the complex conductivity of disordered superconductors under an *arbitrary* dc bias using the Keldysh-Usadel theory of nonequilibrium superconductivity. This formula is relatively simple, making it more accessible to a broader research community. Our analysis reveals that in a strongly dc-biased dirty-limit superconductor, the Higgs mode induces an instability in the homogeneous superflow within a specific frequency window, making the high-current-carrying state vulnerable to ac perturbations. This instability, which occurs exclusively in the ac ∥ dc configuration, leads to a nonmonotonic dependence of kinetic inductance on frequency and bias strength. By carefully tuning the dc bias and the frequency of the ac perturbation, the kinetic inductance can be enhanced by nearly 2 orders of magnitude. In the weak-dc-bias regime, our formula recovers the well-known quadratic dependence, $L_k \propto 1 + C(J_b/J_{\rm dp})^2$, with coefficients $C = 0.409$ for ac ∥ dc and $C = 0.136$ for ac ⊥ dc, where $J_{\rm dp}$ is the equilibrium depairing current density. These findings establish a robust theoretical framework for dc-biased superconducting systems and suggest that Higgs-mode physics could be exploited in the design and optimization of superconducting detectors. Moreover, they may lead to a yet-to-be-explored detector concept based on Higgs-mode physics.

DOI: 10.1103/PhysRevApplied.23.054091

I. INTRODUCTION

A conventional *s*-wave superconductor under a dc bias is a fundamental yet intricate physical system that underpins various applications, including kinetic inductance detectors [1], traveling-wave parametric amplifiers [2], neutron detector [3], single-photon detectors [4], superconducting diodes [5], and the fundamental study of superconducting rf cavities for particle accelerators [6]. Although the behavior of a dc-biased superconductor may initially seem straightforward, the introduction of an ac field parallel to the bias (ac ∥ dc) gives rise to highly nontrivial physical phenomena, where the Higgs mode plays a pivotal role [7–10].

The Higgs mode, $\delta\Delta(t)$, corresponds to oscillations in the amplitude of the superconducting order parameter Δ (see, e.g., Refs. [11–22]). It is well known that the Higgs mode couples to electromagnetic fields through a term of the form $\mathbf{A} \cdot \mathbf{A}\delta\Delta$ [Fig. 1(a)], similar to how the Higgs

boson *h* in particle physics couples to the *Z* boson via a *ZZh* interaction. As a result, the Higgs mode typically appears in nonlinear responses and requires strong electromagnetic irradiation to be observed [15,16]. However, when an ac field is superposed on a dc bias, the coupling term becomes $\mathbf{A}_{\rm dc} \cdot \mathbf{A}\delta\Delta$ [7–10], allowing the Higgs mode to respond *linearly* to the electromagnetic field in the ac ∥ dc configuration [Fig. 1(b)]. This effect was first identified by Moor *et al.* [7], who predicted that the Higgs resonance would appear at $\hbar\omega = 2\Delta$ for ac ∥ dc. This prediction was later confirmed experimentally by Nakamura *et al.* [8]. For the ac ⊥ dc configuration [Fig. 1(c)], however, this coupling vanishes. It is worth noting that Budzinski *et al.* [23] seemingly observed the Higgs mode under a dc bias nearly half a century ago using aluminum samples with varying mean free paths (see also the discussion in Ref. [10]).

The pioneering work by Moor *et al.* [7] mainly considered weak dc biases, treating both the ac field and dc bias as small perturbations. However, the *nonperturbative* effects of a strong dc bias on the Higgs resonance and its broader implications remained largely unexplored. To address this,

---

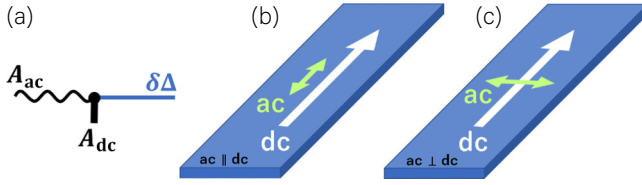*Contact author: kubotaka@post.kek.jp

054091-1

FIG. 1. (a) A schematic illustration of the Higgs-mode inter-action with the electromagnetic field. When an ac field is super-posed on a bias dc in parallel, the bias dc acts as a tuning knob, enabling the Higgs mode to respond linearly and be amplified. (b),(c) A narrow superconducting thin film under a bias dc with a superposed ac field in the (b) ac ∥ dc and (c) ac ⊥ dc configura-tions. In the ac ∥ dc case, the Higgs mode responds linearly to the ac perturbation, whereas in the ac ⊥ dc case, no such response occurs.

Jujo [9] developed a general theoretical framework based on the Keldysh-Eilenberger formalism to compute the sur-face resistance of superconductors with arbitrary mean free path and bias dc strength. Expanding upon this frame-work, Ref. [10] computed the complex conductivity over a wide range of bias current strengths, ac-perturbation frequencies, and temperatures, revealing that the Higgs-mode contribution is not only significant near $\hbar\omega \simeq 2\Delta$ but also at $\hbar\omega \ll \Delta$, a frequency range directly relevant to superconducting devices.

Among the key findings of Ref. [10], one of the most striking results is the profound impact of the Higgs mode on the bias-dependent kinetic inductance $L_k(J_b)$. The coef-ficient C in the low-bias expansion,

$$L_k(J_b) = L_k(0) \left[1 + C \left(\frac{J_b}{J_{\mathrm{dp}}} \right)^2 + \dots \right], \qquad (1)$$

where J_{dp} is the equilibrium depairing current density, was numerically determined for various mean free paths and temperatures. For the ac ∥ dc configuration, C was found to approach $C \simeq 0.4$ as the mean free path decreases. On the other hand, C for the ac ⊥ dc configuration, obtained by omitting nonequilibrium corrections due to the ac per-turbation, approaches $C \simeq 0.14$.

Notably, these numerical results align with previous analytical studies of $L_k(J_b)$, where C was derived using the equilibrium Usadel equation combined with one of the following phenomenological assumptions about nonequi-librium effects: (i) the *oscillating n_s assumption*, in which the superfluid density (n_s) oscillates in sync with the alter-nating current, leading to $C(T \to 0) \simeq 0.409$ [24,25]; and (ii) the *frozen-n_s assumption*, in which the superfluid den-sity remains fixed at its equilibrium value set by the dc bias, yielding $C(T \to 0) \simeq 0.136$ [24].

These phenomenological assumptions [24–27] were his-torically motivated by the idea that if the ac frequency is lower than the inverse relaxation time of the superfluid

density, n_s will oscillate along with the ac; conversely, if the ac frequency is higher, n_s will remain fixed at its equilibrium value, determined by the strength of the bias dc. Thus, these assumptions were referred to as the *slow-experiment* and *fast-experiment* assumptions. However, it is now evident that the distinction between these regimes is not determined by whether the ac frequency is slow or fast but, rather, by whether the Higgs mode is excited (ac ∥ dc) or remains inactive (ac ⊥ dc).

Despite these advancements, initiated by the pioneering work of Moor *et al.* [7], we can expect that some intriguing phenomena remain hidden. These would arise in a dirty-limit superconductor under a strong bias dc comparable to J_{dp}, because the Higgs resonance becomes increasingly pronounced as the mean free path shortens and the dc bias is strengthened [9,10]. This provides an ideal setting in which Higgs-mode physics is most prominent. Coin-cidentally, this is also the operating regime of various superconducting applications.

There are several challenges and open questions. (i) The complex-conductivity formula for a dirty-limit super-conductor under an arbitrary bias dc, which is crucial for investigating this regime, has yet to be established. While a more general expression covering the entire range from the dirty to clean limit has been derived using the Keldysh-Eilenberger formalism [9,10], a specialized for-mula for the dirty limit is expected to be significantly simpler. Such a formulation would not only provide deeper physical insight but also make the theoretical framework more accessible to a broader range of researchers. (ii) Does the stability of the homogeneous superflow persist in the presence of a strong Higgs resonance (i.e., oscilla-tions of the superfluid density), particularly as the mean free path decreases and the dc bias increases? (iii) In the previous study [10], the coefficient C was numeri-cally computed but its exact analytical value in the dirty limit remains undetermined. Do these values exactly coin-cide with those previously obtained under the oscillating and frozen superfluid density assumptions? (iv) How does bias-dependent kinetic inductance behave under strong dc bias in a dirty-limit superconductor, where the Higgs res-onance is pronounced, and can these effects be leveraged for designing and optimizing superconducting devices?

In this paper, we address these outstanding issues using the Keldysh-Usadel theory of nonequilibrium supercon-ductivity. The paper is organized as follows. In Sec. II, we derive the complex-conductivity formula for a disordered superconductor subjected to an ac perturbation superposed on a bias dc of arbitrary strength. In Sec. III, we apply this formula to investigate the Higgs-mode contribution to the complex conductivity and examine the stability of the homogeneous superflow. In Sec. IV, we analyze the bias-dependent kinetic inductance. Finally, in Sec. V we sum-marize our findings and discuss their broader implications, including superconducting-device applications. Readers

unfamiliar with the theoretical methods used in this paper may skip Secs. II, III, and IV and proceed directly to Sec. V.

II. FORMULATION

The purpose of this section is to derive the complex-conductivity formula for a disordered superconductor under an arbitrary bias dc strength, starting from the Keldysh-Usadel equations.

A. Keldysh-Usadel equations

We examine the behavior of a narrow thin-film superconductor, subjected to a bias dc current of arbitrary magnitude that flows parallel to the strip. Superimposed on this is a weak electromagnetic field. The formalism used is the Keldysh-Usadel quasiclassical Green's functions (see, e.g., Refs. [28–30]), which is a well-established approach for analyzing nonequilibrium superconductivity in the dirty limit, where the dependence on the Fermi-momentum direction $\hat{\mathbf{p}}_f$ vanishes as elastic scattering rapidly isotropizes the momentum. In this framework, the quasiclassical Green's functions are expressed in a mixed Fourier representation with retarded, advanced, and Keldysh components, denoted by $\hat{g}^{R,A,K}(\mathbf{R}, \epsilon, t)$. Since the film is uniform across its width and thickness, the spatial variable $\mathbf{R}$ reduces to a single coordinate along the longitudinal direction of the film. These are 2×2 matrix functions in Nambu space. The governing equations for the retarded (R) and advanced (A) components of the Green's functions are given by

$$i\hbar D \hat{\partial} \circ \left\{ \hat{g}^r \circ (\hat{\partial} \circ \hat{g}^r) \right\} = [\epsilon \hat{\tau}_3 + \hat{\Delta}, \hat{g}^r]_\circ \quad (r = R, A),$$

(2)

$$\hat{g}^R \circ \hat{g}^R = \hat{g}^A \circ \hat{g}^A = 1,$$

(3)

where D is the diffusion constant, $\hat{\tau}_3$ is the third Pauli matrix, and $\hat{\Delta}$ represents the superconducting gap. The Keldysh component $\hat{g}^K$ satisfies similar equations:

$$i\hbar D \hat{\partial} \circ \left\{ \hat{g}^R \circ (\hat{\partial} \circ \hat{g}^K) + \hat{g}^K \circ (\hat{\partial} \circ \hat{g}^A) \right\} = [\epsilon \hat{\tau}_3 + \hat{\Delta}, \hat{g}^K]_\circ,$$

(4)

$$\hat{g}^R \circ \hat{g}^K + \hat{g}^K \circ \hat{g}^A = 0.$$

(5)

The "$\circ$" product here refers to the Moyal product, defined as $X \circ Y = \exp\left[(i\hbar/2)\left(\partial_\epsilon^X \partial_t^Y - \partial_t^Y \partial_\epsilon^X\right)\right] XY$, while $[X, Y]_\circ$ represents the commutator in this context. Under the influence of a gauge-invariant superfluid momentum $\hbar \mathbf{q} = \hbar \nabla \chi - 2e\mathbf{A}$, the operator $\hat{\partial} \circ$ reduces to $\hat{\partial} \circ \hat{g}^{R,A,K} = (i/2)[\hat{\tau}_3 \mathbf{q}, \hat{g}]_\circ$ (see, e.g., Ref. [30]). The gap equation governing the superconducting order parameter Δ is derived

from the Keldysh component and is expressed as

$$\Delta(t) = -\frac{\mathscr{G}}{8} \int d\epsilon \, \mathrm{Tr}[(-i\tau_2)\hat{g}^K(\epsilon, t)],$$

(6)

where $\mathscr{G}$ is the BCS coupling constant. The current density $\mathbf{J}(t)$ in the superconductor is given by

$$\mathbf{J}(t) = -i\frac{\sigma_n}{e} \int d\epsilon \mathbf{S}(\epsilon, t),$$

(7)

$$\mathbf{S}(\epsilon, t) = \frac{i}{8}\mathrm{Tr}\left[\hat{\tau}_3 \left\{\hat{g}^R \circ (\hat{\partial} \circ \hat{g}^K) + \hat{g}^K \circ (\hat{\partial} \circ \hat{g}^A)\right\}\right],$$

(8)

where $\sigma_n = 2e^2 N_0 D$ is the normal conductivity and N_0 is the normal density of states at the Fermi level.

Equations (2)–(8) form the general framework of the Keldysh-Usadel formalism for nonequilibrium superconductivity. From this framework, we analyze the linear response to a weak electromagnetic field in the presence of a dc bias of arbitrary strength.

B. Linear response to a weak electromagnetic field in the presence of a bias dc of arbitrary strength

We define the total momentum as $\mathbf{q} = \mathbf{q}_b + \delta\mathbf{q}(t)$, where $\mathbf{q}_b$ represents the constant bias momentum due to the dc component. The strength of $\mathbf{q}_b$ can vary from zero up to the depairing momentum. The term $\delta\mathbf{q}(t)$ denotes the time-dependent perturbation applied to the system.

In this framework, the Green's functions $\hat{g}^{R,A,K}(\epsilon, t)$ are decomposed as $\hat{g}^{R,A,K}(\epsilon, t) = \hat{g}_b^{R,A,K}(\epsilon) + \delta\hat{g}^{R,A,K}(\epsilon, t)$, where $\hat{g}_b^{R,A,K}(\epsilon)$ represents the equilibrium component in the presence of the dc bias and $\delta\hat{g}^{R,A,K}(\epsilon, t)$ accounts for the perturbative response. Similarly, the superconducting order parameter is expressed as $\hat{\Delta}(t) = \hat{\Delta}_b + \delta\hat{\Delta}(t)$, with $\hat{\Delta}_b$ representing the bias-induced equilibrium value, and $\delta\hat{\Delta}(t)$ represents the time-dependent fluctuation of the order parameter, the Higgs mode. This decomposition allows us to reformulate Eqs. (2)–(8) in terms of orders of approximation.

The zeroth-order equations, which describe the equilibrium Green's functions for an arbitrary strength of dc bias, take the following form:

$$-i(s/2)\left\{\hat{\tau}_3 \hat{g}_b^r(\epsilon)\hat{\tau}_3 \hat{g}_b^r(\epsilon) - \hat{g}_b^r(\epsilon)\hat{\tau}_3 \hat{g}_b^r(\epsilon)\hat{\tau}_3\right\}$$
$$= \left[\epsilon\hat{\tau}_3 + \hat{\Delta}_b, \hat{g}_b^r(\epsilon)\right],$$

(9)

$$\hat{g}_b^K(\epsilon) = \left\{\hat{g}_b^R(\epsilon) - \hat{g}_b^A(\epsilon)\right\} \mathcal{T}(\epsilon),$$

(10)

$$\Delta_b = -\frac{\mathscr{G}}{8}\int d\epsilon \, \mathrm{Tr}\left[(-i\hat{\tau}_2)\hat{g}_b^K(\epsilon)\right],$$

(11)

with the normalization condition $\hat{g}_b^r(\epsilon)\hat{g}_b^r(\epsilon) = 1$ and $\hat{g}_b^R(\epsilon)\hat{g}_b^K(\epsilon) + \hat{g}_b^K(\epsilon)\hat{g}_b^A(\epsilon) = 0$, where

$$s := \frac{\hbar D}{2}q_b^2 \tag{12}$$

represents the strength of the bias superflow and $\mathcal{T}(\epsilon) := \tanh(\epsilon/2kT) = 1 - 2f_{\mathrm{FD}}(\epsilon)$ is the equilibrium distribution function, with $f_{\mathrm{FD}}(\epsilon)$ representing the Fermi-Dirac distribution. These equations describe the equilibrium Green's functions in the presence of a bias dc and are applicable to bias dc of any strength.

At the first-order approximation with respect to the weak ac field, the equations governing the R and A components of the perturbed Green's functions, $\delta\hat{g}^r(\epsilon,\omega)$ ($r = R, A$), in Fourier space are given by

$$
\begin{aligned}
&- i(s/2)\left\{\hat{\tau}_3\hat{g}_b^r(\epsilon_+)\hat{\tau}_3\delta\hat{g}^r(\epsilon,\omega) - \hat{g}_b^r(\epsilon_+)\hat{\tau}_3\delta\hat{g}^r(\epsilon,\omega)\hat{\tau}_3\right.\\
&\quad + \hat{\tau}_3\delta\hat{g}^r(\epsilon,\omega)\hat{\tau}_3\hat{g}_b^r(\epsilon_-) - \delta\hat{g}^r(\epsilon,\omega)\hat{\tau}_3\hat{g}_b^r(\epsilon_-)\hat{\tau}_3\left.\right\}\\
&\quad - i(\delta W/2)\left\{\hat{\tau}_3\hat{g}_b^r(\epsilon_+)\hat{\tau}_3\hat{g}_b^r(\epsilon_-)\right.\\
&\quad - \hat{g}_b^r(\epsilon_+)\hat{\tau}_3\hat{g}_b^r(\epsilon_-)\hat{\tau}_3 + \hat{\tau}_3\hat{g}_b^r(\epsilon_-)\hat{\tau}_3\hat{g}_b^r(\epsilon_-)\\
&\quad - \hat{g}_b^r(\epsilon_+)\hat{\tau}_3\hat{g}_b^r(\epsilon_+)\hat{\tau}_3\left.\right\} = \epsilon_+\hat{\tau}_3\delta\hat{g}^r(\epsilon,\omega) - \delta\hat{g}^r(\epsilon,\omega)\hat{\tau}_3\epsilon_-\\
&\quad + [\hat{\Delta}_b, \delta\hat{g}^r(\epsilon,\omega)] + \delta\hat{\Delta}(\omega)\hat{g}_b^r(\epsilon_-) - \hat{g}_b^r(\epsilon_+)\delta\hat{\Delta}(\omega),
\end{aligned}
\tag{13}
$$

with the normalization condition

$$\hat{g}_b^r(\epsilon_+)\delta\hat{g}^r(\epsilon,\omega) + \delta\hat{g}^r(\epsilon,\omega)\hat{g}_b^r(\epsilon_-) = 0, \tag{14}$$

where $\delta W = (\hbar D/2)\mathbf{q}_b \cdot \delta\mathbf{q}_\omega$, $\delta\mathbf{q}_\omega = \int \delta\mathbf{q}(t)e^{i\omega t}dt$ is the Fourier transform of the ac field $\delta\mathbf{q}(t)$ and $\epsilon_\pm = \epsilon \pm \hbar\omega/2$. The equation for the Keldysh component in Fourier space, $\delta\hat{g}^K(\epsilon,\omega)$, is given by

$$
\begin{aligned}
&- i(s/2)\left[\hat{\tau}_3\hat{g}_b^R(\epsilon_+)\hat{\tau}_3\delta\hat{g}^K(\epsilon,\omega) - \hat{g}_b^R(\epsilon_+)\hat{\tau}_3\delta\hat{g}^K(\epsilon,\omega)\hat{\tau}_3\right.\\
&\quad + \hat{\tau}_3\delta\hat{g}^R(\epsilon,\omega)\hat{\tau}_3\hat{g}_b^K(\epsilon_-) - \delta\hat{g}^R(\epsilon,\omega)\hat{\tau}_3\hat{g}_b^K(\epsilon_-)\hat{\tau}_3\\
&\quad + \hat{\tau}_3\hat{g}_b^K(\epsilon_+)\hat{\tau}_3\delta\hat{g}^A(\epsilon,\omega) - \hat{g}_b^K(\epsilon_+)\hat{\tau}_3\delta\hat{g}^A(\epsilon,\omega)\hat{\tau}_3\\
&\quad + \hat{\tau}_3\delta\hat{g}^K(\epsilon,\omega)\hat{\tau}_3\hat{g}_b^A(\epsilon_-) - \delta\hat{g}^K(\epsilon,\omega)\hat{\tau}_3\hat{g}_b^A(\epsilon_-)\hat{\tau}_3\left.\right]\\
&\quad - i(\delta W/2)\left[\hat{\tau}_3\hat{g}_b^R(\epsilon_+)\hat{\tau}_3\hat{g}_b^K(\epsilon_-) - \hat{g}_b^R(\epsilon_+)\hat{\tau}_3\hat{g}_b^K(\epsilon_-)\hat{\tau}_3\right.\\
&\quad + \hat{\tau}_3\hat{g}_b^R(\epsilon_-)\hat{\tau}_3\hat{g}_b^K(\epsilon_-) - \hat{g}_b^R(\epsilon_+)\hat{\tau}_3\hat{g}_b^K(\epsilon_+)\hat{\tau}_3\\
&\quad + \hat{\tau}_3\hat{g}_b^K(\epsilon_+)\hat{\tau}_3\hat{g}_b^A(\epsilon_-) - \hat{g}_b^K(\epsilon_+)\hat{\tau}_3\hat{g}_b^A(\epsilon_-)\hat{\tau}_3\\
&\quad + \hat{\tau}_3\hat{g}_b^K(\epsilon_-)\hat{\tau}_3\hat{g}_b^A(\epsilon_-) - \hat{g}_b^K(\epsilon_+)\hat{\tau}_3\hat{g}_b^A(\epsilon_+)\hat{\tau}_3\left.\right]\\
&= \epsilon_+\hat{\tau}_3\delta\hat{g}^K(\epsilon,\omega) - \delta\hat{g}^K(\epsilon,\omega)\hat{\tau}_3\epsilon_-\\
&\quad + [\hat{\Delta}_b, \delta\hat{g}^K(\epsilon,\omega)] + \delta\hat{\Delta}(\omega)\hat{g}_b^K(\epsilon_-) - \hat{g}_b^K(\epsilon_+)\delta\hat{\Delta}(\omega).
\end{aligned}
\tag{15}
$$

The corresponding normalization condition is

$$
\begin{aligned}
&\hat{g}_b^R(\epsilon_+)\delta\hat{g}^K(\epsilon,\omega) + \delta\hat{g}^K(\epsilon,\omega)\hat{g}_b^A(\epsilon_-)\\
&\quad + \hat{g}_b^K(\epsilon_+)\delta\hat{g}^A(\epsilon,\omega) + \delta\hat{g}^R(\epsilon,\omega)\hat{g}_b^K(\epsilon_-) = 0.
\end{aligned}
\tag{16}
$$

From the gap equation, we derive

$$\delta\Delta(\omega) = -\frac{\mathcal{G}}{8}\int d\epsilon \, \mathrm{Tr}[(-i\tau_2)\delta\hat{g}^K(\epsilon,\omega)]. \tag{17}$$

The current density induced by the perturbative ac field is given by

$$\delta\mathbf{J}(\omega) = -i\frac{\sigma_n}{e}\int d\epsilon \, \delta\mathbf{S}(\epsilon,\omega), \tag{18}$$

$$
\begin{aligned}
\delta\mathbf{S}(\epsilon,\omega) = (i/16)\mathrm{Tr}\,[i\mathbf{q}_b\\
\times\left\{\hat{\tau}_3\hat{g}_b^R(\epsilon_+)\hat{\tau}_3\delta\hat{g}^K(\epsilon,\omega) + \hat{\tau}_3\delta\hat{g}^R(\epsilon,\omega)\hat{\tau}_3\hat{g}_b^K(\epsilon_-)\right.\\
+ \hat{\tau}_3\hat{g}_b^K(\epsilon_+)\hat{\tau}_3\delta\hat{g}^A(\epsilon,\omega) + \hat{\tau}_3\delta\hat{g}^K(\epsilon,\omega)\hat{\tau}_3\hat{g}_b^A(\epsilon_-)\left.\right\}\\
+ i\delta\mathbf{q}_\omega\left\{\hat{\tau}_3\hat{g}_b^R(\epsilon_+)\hat{\tau}_3\hat{g}_b^K(\epsilon_-) + \hat{\tau}_3\hat{g}_b^K(\epsilon_+)\hat{\tau}_3\hat{g}_b^A(\epsilon_-)\right\}\left.\right].
\end{aligned}
\tag{19}
$$

By comparing this with $\delta\mathbf{J} = \sigma\delta\mathbf{E} = -i\sigma\hbar\omega\delta\mathbf{q}_\omega/e$, the complex conductivity σ can be evaluated.

With this, all the equations are now in place. Using Eqs. (9)–(17), we can determine $\hat{g}_b^{R,A,K}$, $\delta\hat{g}^{R,A,K}$, and $\delta\hat{\Delta}$, which allows us to calculate the complex conductivity σ via Eqs. (18) and (19). In the following subsections, this process is carried out step by step by expressing all components within the matrices as follows: $\hat{\Delta} = i\hat{\tau}_2\Delta$, $\hat{g}^R = \hat{\tau}_3 G + i\hat{\tau}_2 F$, and $\hat{g}^A = -\hat{\tau}_3\hat{g}^{R\dagger}\hat{\tau}_3$. In Sec. II C, we solve the zeroth-order equations to obtain $\hat{g}_b^{R,A,K}$. In Sec. II D, we then address the first-order equations to derive $\delta\hat{g}^{R,A,K}$ and $\delta\hat{\Delta}$. In Sec. II E, we derive the complex-conductivity formula.

C. Equilibrium Green's functions in the presence of an arbitrary strength of bias dc

The zeroth-order equation [Eq. (9)] simplifies to the well-known dc-carrying Usadel equation: $\Delta_b G_b - \epsilon F_b = isG_bF_b$. By numerically solving this equation for a given s, we construct a table of $G_b(\epsilon)$ and $F_b(\epsilon)$ for all relevant ϵ values. These results are essential for calculating the nonequilibrium Green's functions and the Higgs mode in Sec. II D, as well as the complex conductivity in Sec. II E. Although this equation has been solved in numerous studies over the past decades, we provide a brief explanation of our solution method here for the reader's convenience.

We begin by converting the Usadel equation into the Matsubara representation:

$$\Delta_b G_m - \hbar\omega_m F_m = s G_m F_m, \qquad (20)$$

where $G_m = G_b(i\hbar\omega_m)$, $F_m = iF_b(i\hbar\omega_m)$, and $\hbar\omega_m = 2\pi kT(m + 1/2)$ is the Matsubara frequency. The normalization condition in the Matsubara representation becomes $G_m^2 + F_m^2 = 1$. The order parameter Δ_b under a bias dc is determined by the gap equation [Eq. (11)], which can also be expressed as

$$\ln\frac{T_{c0}}{T} = 2\pi kT \sum_{\omega_m > 0}\left(\frac{1}{\hbar\omega_m} - \frac{F_m}{\Delta_b}\right). \qquad (21)$$

Solving Eqs. (20) and (21) to determine Δ_b, G_m, and F_m is a straightforward task. Once these quantities are obtained, the bias dc current can be calculated using the following relations:

$$\frac{J_b(s,T)}{J_0} = \sqrt{\pi\frac{s}{\Delta_0}}\frac{n_s(s,T)}{n_{s0}}, \qquad (22)$$

$$\frac{n_s(s,T)}{n_{s0}} = \frac{\lambda_0^2}{\lambda^2(s,T)} = \frac{4kT}{\Delta_0}\sum_{\omega_m > 0} F_m^2. \qquad (23)$$

Here, $J_0 = H_{c0}/\lambda_0$, $n_{s0} = 2\pi m N_0 D\Delta_0/\hbar$, $\lambda_0 = \lambda(0,0) = \sqrt{\hbar/\pi\mu_0\Delta_0\sigma_n}$, and $H_{c0} = \sqrt{N_0/\mu_0}\Delta_0$. Note that Eq. (22) provides the relationship between the bias superflow parameter s and the bias current J_b, which is essential for translating results expressed as a function of s into those expressed as a function of J_b (see also Appendix A).

In Fig. 2(a), we depict the bias dc (J_b) as a function of the normalized bias momentum $q_b/q_\xi = \sqrt{s/\Delta_0}$, providing a means to translate momentum into current. The dot indicates the well-known dirty-limit equilibrium depairing current density, $J_{dp}(0) = 0.595 H_{c0}/\lambda_0$, derived decades ago [31–33] (see also Appendix A). In Fig. 2(b), we show the pair potential Δ_b under a bias dc as a function of J_b, up to the depairing current density (blue curve).

Having determined Δ_b for a given s through the Matsubara-representation calculations described above, solving the real-frequency representation of the Usadel equation to obtain the equilibrium Green's functions under a bias dc (G_b and F_b) becomes straightforward. First, the spectral gap, defined as the maximum energy ϵ for which the quasiparticle density of states vanishes, is given by [31,32]

$$\epsilon_g = \left(\Delta_b^{\frac{2}{3}} - s^{\frac{2}{3}}\right)^{\frac{3}{2}}, \qquad (24)$$

and is illustrated in Fig. 2(b) (black curve). To calculate the spectrum, we rewrite the real-frequency representation of the Usadel equation using the parametrization $G_b = \cosh(u + iv)$ and $F_b = \sinh(u + iv)$, which transforms the problem into two equations for u and v:

$$s(\epsilon\cosh u + \Delta_b\sinh u)\cos^3 v + \Gamma\epsilon\cos^2 v$$
$$- s\left(\epsilon\cosh^3 u - \Delta_b\sinh^3 u\right)\cos v$$
$$- \Gamma\cosh u \cdot (\epsilon\cosh u - \Delta_b\sinh u) = 0, \qquad (25)$$

$$s\cos v\cosh^3 u + \Gamma\cosh^2 u - s\cos^3 v\cosh u$$
$$+ (\Delta_b\sin v - \Gamma\cos v)\cos v = 0. \qquad (26)$$

Here, Γ represents a small damping factor (e.g., $\Gamma/\Delta_0 = 10^{-5}$), introduced to stabilize the numerical computation and facilitate convergence.

The solutions to Eqs. (25) and (26) can be obtained in a straightforward manner. Representative examples of G_b and F_b calculated using this method are shown in Figs. 2(c) and 2(d), respectively. Furthermore, it is easy to confirm that the spectral gap ϵ_g determined in Fig. 2(b) aligns consistently with the gap edges presented in Fig. 2(c).

At this stage, we can determine $G_b(\epsilon)$ and $F_b(\epsilon)$ for a given s or J_b. The next step is to express the nonequilibrium Green's functions in terms of $G_b(\epsilon)$ and $F_b(\epsilon)$.
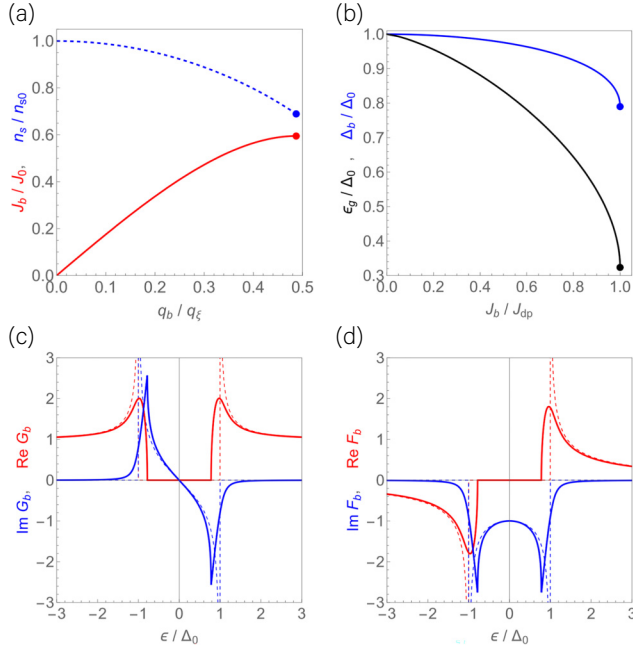

FIG. 2. The equilibrium properties of a superconducting film under a bias dc at zero temperature. (a) The bias dc current density J_b as a function of the bias superfluid momentum q_b. The dot indicates the depairing current density J_{dp}. (b) The pair potential Δ_b (blue) and the spectral gap ϵ_g (black) as functions of the bias dc current density J_b. The dot indicates the equilibrium depairing current density J_{dp}. (c) The real and imaginary parts of G_b for $J_b = 0$ (dashed) and $J_b = 0.6J_{dp}$ (solid). (d) The real and imaginary parts of F_b for $J_b = 0$ (dashed) and $J_b = 0.6J_{dp}$ (solid).

D. Nonequilibrium Green's functions and the Higgs mode

Our next task is to solve the first-order equations for the $R(A)$ and K components [Eqs. (13) and (15)]. Although the calculations are lengthy, they are straightforward and yield relatively simple solutions expressed in terms of G_b and F_b.

The first-order equation of the $R(A)$ component [Eq. (13)] and the normalization condition [Eq. (14)] lead to

$$\delta G(\epsilon, \omega) = \frac{F_{b+} + F_{b-}}{G_{b+} + G_{b-}} \delta F(\epsilon, \omega), \qquad (27)$$

$$\delta F(\epsilon, \omega) = \zeta \delta \Delta(\omega) + \kappa \delta W, \qquad (28)$$

$$\zeta = -\frac{G_{b+} + G_{b-}}{\hbar \omega} \frac{F_{b+} - F_{b-}}{F_{b+} + F_{b-}}, \qquad (29)$$

$$\kappa = i \frac{G_{b+} + G_{b-}}{\hbar \omega} (F_{b+} - F_{b-}), \qquad (30)$$

where $G_{b\pm} = G_b(\epsilon \pm \hbar\omega/2)$ and $F_{b\pm} = F_b(\epsilon \pm \hbar\omega/2)$.

The first-order equation of the K component [Eq. (15)] and the normalization condition [Eq. (16)] can be solved by expressing $\delta\hat{g}^K$ in terms of the *anomalous* term $\delta\hat{g}^a$, following Eliashberg's approach [34,35]:

$$\delta\hat{g}^K = \delta\hat{g}^R \mathcal{T}_- - \delta\hat{g}^A \mathcal{T}_+ + \delta\hat{g}^a (\mathcal{T}_+ - \mathcal{T}_-). \qquad (31)$$

Substituting this form and performing a lengthy calculation, we obtain

$$\delta G^a(\epsilon, \omega) = \frac{F_{b+} - F_{b-}^*}{G_{b+} - G_{b-}^*} \delta F^a(\epsilon, \omega), \qquad (32)$$

$$\delta F^a(\epsilon, \omega) = \zeta^a \delta\Delta + \kappa^a \delta W, \qquad (33)$$

$$\zeta^a = -\frac{G_{b+} - G_{b-}^*}{\hbar\omega} \frac{F_{b+} + F_{b-}^*}{F_{b+} - F_{b-}^*}, \qquad (34)$$

$$\kappa^a = i \frac{G_{b+} - G_{b-}^*}{\hbar\omega} (F_{b+} + F_{b-}^*). \qquad (35)$$

With $\delta\hat{g}^K$ now expressed in terms of G_b, F_b, δW, and $\delta\Delta$, we substitute it into the perturbative part of the gap equation [Eq. (17)]. This yields

$$\delta\Delta(\omega) = \Psi \delta W, \qquad (36)$$

$$\Psi = \frac{-(\mathscr{G}/4) \int d\epsilon\, \psi_N(\epsilon)}{1 + (\mathscr{G}/4) \int d\epsilon\, \psi_D(\epsilon)}, \qquad (37)$$

$$\psi_N = \kappa \mathcal{T}_- + \kappa^* \mathcal{T}_+ + (\mathcal{T}_+ - \mathcal{T}_-)\kappa^a, \qquad (38)$$

$$\psi_D = \zeta \mathcal{T}_- + \zeta^* \mathcal{T}_+ + (\mathcal{T}_+ - \mathcal{T}_-)\zeta^a. \qquad (39)$$

Note that in the ac $\perp$ dc (i.e., $\delta\mathbf{q} \perp \mathbf{q}_b$) configuration, $\delta W \propto \mathbf{q}_b \cdot \delta\mathbf{q}_\omega$ vanishes. As a result, all nonequilibrium

corrections, including δG, δF, δG^a, δF^a, and $\delta\Delta$, are eliminated.

At this stage, we have solved the Keldysh-Usadel equation and expressed the solution in terms of G_b and F_b for an arbitrary strength of the bias dc. A crucial sanity check, performed by taking the weak-bias dc limit, verifies that our results are fully consistent with the earlier study by Moor *et al.* [7], where both the ac and dc fields were treated as perturbations (see Appendix B). Furthermore, in the short-mean-free-path limit, our results correspond to those obtained in the more general framework of Refs. [9,10], which considered arbitrary mean free paths.

The next step is to derive an explicit expression for the complex-conductivity formula based on these solutions.

E. Complex conductivity under a weak ac field superposed on an arbitrary strength of bias dc

We examine two specific configurations: one in which the ac perturbation is parallel to the dc bias (ac $\parallel$ dc, i.e., $\delta\mathbf{q} \parallel \mathbf{q}_b$), and the other in which it is perpendicular (ac $\perp$ dc, i.e., $\delta\mathbf{q} \perp \mathbf{q}_b$). By substituting the nonequilibrium Green's functions [Eqs. (27)–(39)] into the expression for the current response, we arrive at one of the main results of this paper: $\sigma = (\sigma_n/\hbar\omega) \int d\epsilon (\delta S/\delta q_\omega)$ or

$$\sigma = \begin{cases} \sigma^{(0)} + \sigma^{(1)} + \sigma^{(2)} & (\text{ac} \parallel \text{dc}), \\ \sigma^{(0)} & (\text{ac} \perp \text{dc}), \end{cases} \qquad (40)$$

where

$$\frac{\sigma^{(0)}}{\sigma_n} = \int \frac{d\epsilon}{\hbar\omega} (\operatorname{Re} G_b \operatorname{Re} G_b' + \operatorname{Re} F_b \operatorname{Re} F_b')(f_{\text{FD}} - f_{\text{FD}}')$$
$$+ i \int \frac{d\epsilon}{\hbar\omega} (\operatorname{Re} G_b \operatorname{Im} G_b' + \operatorname{Re} F_b \operatorname{Im} F_b')(2f_{\text{FD}} - 1), \qquad (41)$$

$$\frac{\sigma^{(1)}}{\sigma_n} = \frac{8s}{\hbar\omega} \int \frac{d\epsilon}{\hbar\omega} \operatorname{Re} F_b \operatorname{Im} F_b \operatorname{Re} G_b' (f_{\text{FD}} - f_{\text{FD}}')$$
$$+ i \frac{2s}{\hbar\omega} \int \frac{d\epsilon}{\hbar\omega} \big[2 \operatorname{Re} F_b \operatorname{Im} F_b \operatorname{Im} \{G_b + G_b'\} + \big\{ (\operatorname{Re} F_b')^2 - (\operatorname{Re} F_b)^2 + (\operatorname{Im} F_b)^2 - (\operatorname{Im} F_b')^2 \big\} \operatorname{Re} G_b \big] (2f_{\text{FD}} - 1), \qquad (42)$$

$$\frac{\sigma^{(2)}}{\sigma_n} = \frac{2s\Psi}{\hbar\omega} \int \frac{d\epsilon}{\hbar\omega} (\operatorname{Re} F_b \operatorname{Re} G_b' - \operatorname{Re} G_b \operatorname{Re} F_b')$$
$$\times (f_{\text{FD}} - f_{\text{FD}}') + i \frac{2s\Psi}{\hbar\omega} \int \frac{d\epsilon}{\hbar\omega} \big\{ \operatorname{Re} G_b \operatorname{Im}(F_b - F_b') + \operatorname{Re} F_b \operatorname{Im}(G_b + G_b') \big\} (2f_{\text{FD}} - 1). \qquad (43)$$

Here, G_b', F_b', and f_{FD}' denote $G_b(\epsilon + \hbar\omega)$, $F_b(\epsilon + \hbar\omega)$, and $f_{\text{FD}}(\epsilon + \hbar\omega)$, respectively. The functions G_b and F_b are the equilibrium Green's functions under a bias dc, calculated using Eqs. (25) and (26). This formula represents the

dirty-limit counterpart of the previously derived expression [9,10] applicable to arbitrary mean free paths using the Keldysh-Eilenberger theory and is significantly simpler by comparison.

It is worth noting that $\sigma^{(0)}$ closely resembles the well-known formula for the complex conductivity in the absence of a bias dc [36–38]. This term represents a straightforward extension of the zero-bias dc case to the finite-bias dc case, incorporating G_b and F_b, which are the equilibrium Green's functions under a bias dc, instead of the zero-current Green's functions. However, a rigorous derivation based on the Keldysh-Usadel equation reveals that this naive extension is incomplete: in the ac $\parallel$ dc configuration, two additional terms, $\sigma^{(1)}$ and $\sigma^{(2)}$, must supplement $\sigma^{(0)}$. Both terms originate from the *Doppler fluctuation of the superflow*, $\delta W \propto \mathbf{q}_b \cdot \delta\mathbf{q}_\omega$, which drives the nonequilibrium corrections to the Green's functions, as described in Eqs. (27)–(39). Although $\sigma^{(1)}$ and $\sigma^{(2)}$ share the same physical origin, a portion of the Doppler-fluctuation contribution reorganizes into a term proportional to the Higgs-mode amplitude Ψ, which we identify as the *Higgs-mode contribution* $\sigma^{(2)}$. As expected, once the Higgs-mode oscillation $\delta\Delta \propto \Psi$ vanishes, the contribution $\sigma^{(2)}$ also disappears.

III. HIGGS MODE AND COMPLEX CONDUCTIVITY UNDER A BIAS DC

A. Sanity check: Effect of perturbative bias dc

As discussed in Sec. I, when an ac field is superposed parallel to a bias dc (ac $\parallel$ dc), the Higgs mode responds linearly to the ac field [see Fig. 1(a) and Eq. (36)], with the bias dc serving as a tuning knob to amplify the Higgs-mode response. The most straightforward way to examine the Higgs-mode contribution is to consider the perturbative bias dc case and calculate $\mathrm{Re}\,\sigma^{(2)}$ and $\mathrm{Im}\,\sigma^{(2)}$ to leading order, $\mathcal{O}(s)$. In this regime, the zero-current Green's functions, $G_0 = (\epsilon + i0)/\sqrt{(\epsilon + i0)^2 - \Delta^2}$ and $F_0 = \Delta/\sqrt{(\epsilon + i0)^2 - \Delta^2}$, can be substituted for G_b and F_b, respectively. This simplified case was studied in the pioneering work by Moor *et al.* [7], who investigated the Higgs mode in dc-biased dirty superconductors, treating both the ac field and the dc bias as perturbations (see Appendix B). In Fig. 3, we show the calculated results for $\sigma^{(2)}$, where the Higgs mode manifests as a characteristic peak and dip at $\hbar\omega = 2\Delta_0$ in $\mathrm{Re}\,\sigma^{(2)}$ and $\mathrm{Im}\,\sigma^{(2)}$, respectively. The negative contribution from $\mathrm{Im}\,\sigma^{(2)}$ for $\hbar\omega < 2\Delta$ is compensated by the much larger positive component $\mathrm{Im}\,\sigma^{(0)}$ under weak to moderately strong dc bias. However, as the dc bias increases further, this cancellation becomes insufficient, allowing the negative contribution from $\sigma^{(2)}$ to dominate and manifest in the total conductivity. This behavior is discussed in more detail in the following section.
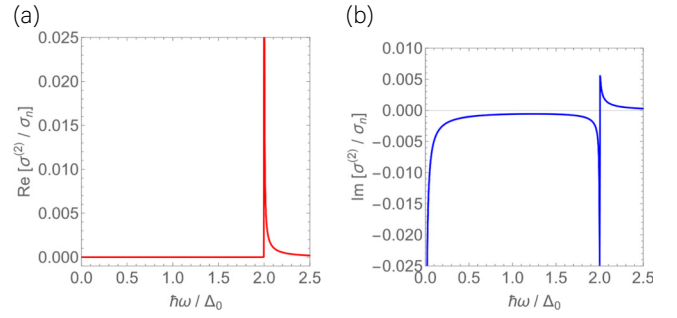

FIG. 3. A sanity check: the manifestation of the Higgs mode in the complex conductivity under a perturbative dc bias. (a),(b) The (a) real and (b) imaginary parts of $\sigma^{(2)}$ calculated for ac $\parallel$ dc, $T = 0$, and $J_b/J_{\mathrm{dp}} \sim q_b/q_\xi = \sqrt{s/\Delta_0} = 0.01$. The effects of a nonperturbative dc bias on the Higgs mode are discussed in Sec. III B and Appendix C.

B. Nonperturbative effects of a strong bias dc and Higgs-induced instability

Now, we explore the impact of stronger bias dc on the complex conductivity, leveraging our previously derived formula [Eqs. (41)–(43)], which remains valid for arbitrary bias dc strengths, including those approaching the depairing current. The calculation procedure is straightforward: numerically compute the equilibrium Green's functions under a bias dc (G_b and F_b) for a given s or J_b using the method outlined in Sec. II C, and substitute them into Eqs. (41)–(43).

To begin with, in Fig. 4 we present the complex conductivity for the ac $\perp$ dc configuration, calculated at $T = 0$. In this configuration, the response is solely determined by $\sigma^{(0)}$. As a result, the complex conductivity exhibits a monotonic dependence on both the frequency and the dc-bias strength, with no Higgs-resonance features. Additionally, the onset of $\mathrm{Re}\,\sigma$ in Fig. 4(a) is given by $\hbar\omega = 2\epsilon_g$, where $\epsilon_g(J_b)$ is shown in Fig. 2(b).
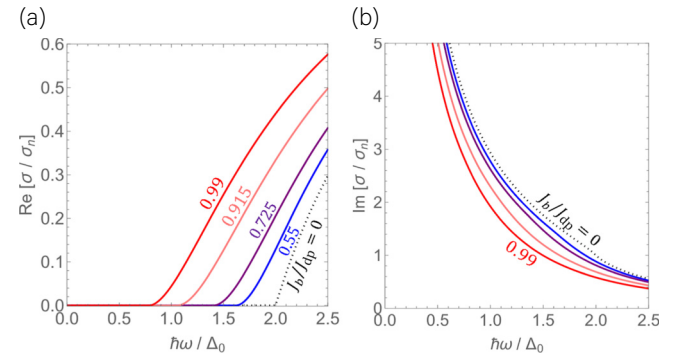

FIG. 4. The absence of Higgs resonance in the complex conductivity for the ac $\perp$ dc configuration. (a),(b) The (a) real part and (b) imaginary parts of the complex conductivity calculated at $T = 0$.

In Fig. 5, we present the real [Figs. 5(a)– 5(d)] and imaginary [Figs. 5(e)– 5(h)] parts of the complex conductivity for the ac ∥ dc configuration, calculated at $T = 0$. For a detailed breakdown of the individual contributions from $\sigma^{(0)}$, $\sigma^{(1)}$, and $\sigma^{(2)}$, see Appendix C. Figures 5(a) and 5(e) correspond to moderately strong dc biases, where the Higgs resonance appears as a peak in Re σ and a dip in Im σ, consistent with the perturbative results shown in Fig. 3. These features become more pronounced as the bias strength increases. However, for even stronger dc biases, the Higgs-mode contribution leads to highly nontrivial dependencies on both frequency and bias strength, as discussed below.

In Figs. 5(b) and 5(f), we illustrate cases with stronger dc biases, ranging from $J_b/J_{dp} = 0.5$ to 0.8, where the Higgs resonance drives Im σ strongly negative. For $J_b/J_{dp} \gtrsim 0.6$, this effect results in two characteristic frequencies:

$$\omega_1(J_b), \omega_2(J_b) \in \{\omega \mid \text{Im}\,\sigma(J_b,\omega) = 0\}. \quad (44)$$

Within the frequency range $\omega_1(J_b) < \omega < \omega_2(J_b)$, Im σ becomes negative. It is well known that a negative kinetic inductance or, equivalently, a negative value of $\omega\,\text{Im}\,\sigma$ [see also Eq. (45)], indicates an instability, as the kinetic energy of the superflow decreases with increasing supercurrent. Thus, within this unstable frequency range, our ansatz of homogeneous solutions to the Keldysh-Usadel equations becomes invalid and the system is expected to

transition into an inhomogeneous state through mechanisms such as phase slips or vortex nucleation [39] (see also Sec. V B).

In Figs. 5(c) and 5(g), we illustrate cases with even stronger dc biases, ranging from $J_b/J_{dp} = 0.85$ to 0.925. For $J_b/J_{dp} = 0.85$ and 0.90, the frequency dependence remains similar to that observed for $J_b/J_{dp} \lesssim 0.8$. However, for $J_b/J_{dp} = 0.925$, the lower bound of the instability frequency window, ω_1, disappears and Im $\sigma(\omega)$ remains negative across the entire low-frequency range below ω_2. This disappearance of ω_1 indicates that the homogeneous current-carrying state becomes unstable against arbitrarily low-frequency ac perturbations as the bias current approaches $J_b/J_{dp} \simeq 0.9$.

As the bias strength increases further, the upper bound of the instability frequency window, ω_2, shifts to lower frequencies and eventually disappears, leading to the complete closure of the instability window. Consequently, the homogeneous current-carrying state regains stability against ac perturbations. In Figs. 5(d) and 5(h), we illustrate this stabilization for $J_b/J_{dp} = 0.99$, with the results for $J_b/J_{dp} = 0.50$ included for comparison.

Interestingly, despite the complex frequency and bias dependence, the onset of Re σ in Figs. 5(a)–5(d) is still given by $\hbar\omega = 2\epsilon_g$, where $\epsilon_g(J_b)$ is shown in Fig. 2(b).

In Fig. 6, we summarize the Higgs-induced instability domain in the ω-J_b plane, based on the calculations presented above. This instability, driven by the Higgs mode, occurs exclusively in the ac ∥ dc configuration and
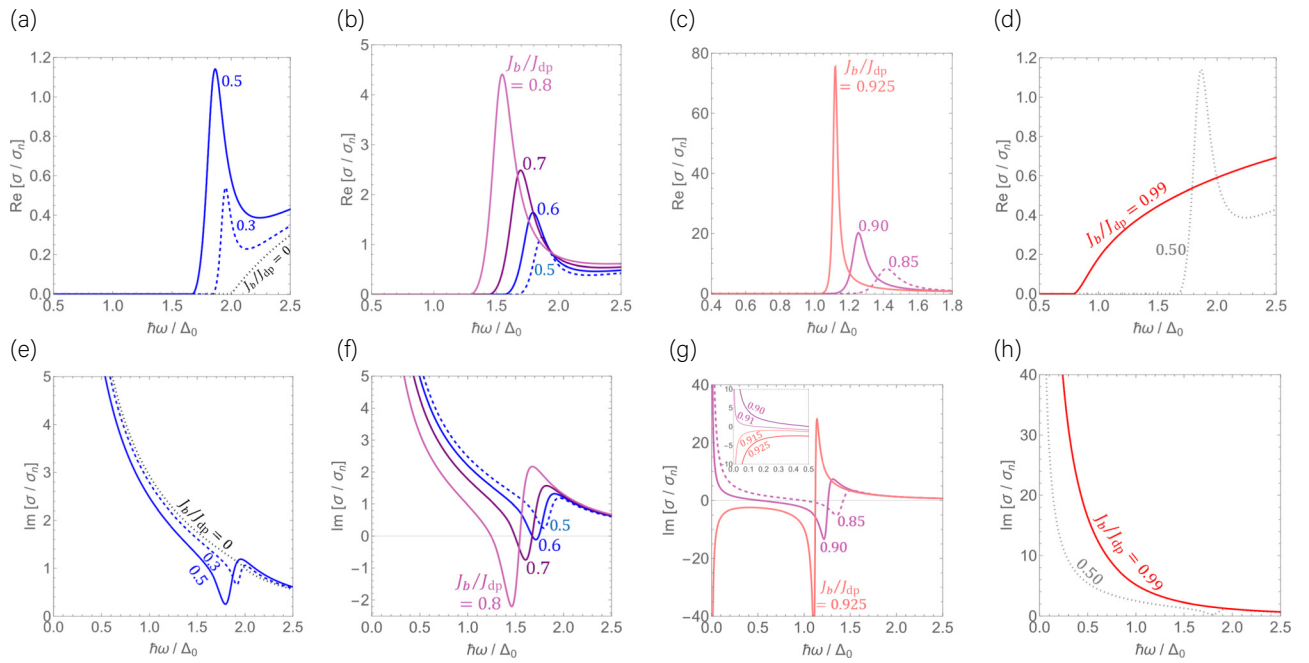

FIG. 5.   The nonperturbative Higgs-mode manifestation in the complex conductivity for the ac ∥ dc configuration under various dc-bias strengths. (a)–(h) The (a)–(d) real and (e)–(h) imaginary parts of the complex conductivity, calculated at $T = 0$. As the bias dc increases, the Higgs resonance becomes more pronounced, leading to nontrivial frequency and bias dependencies, including the onset of instability at sufficiently strong bias currents.
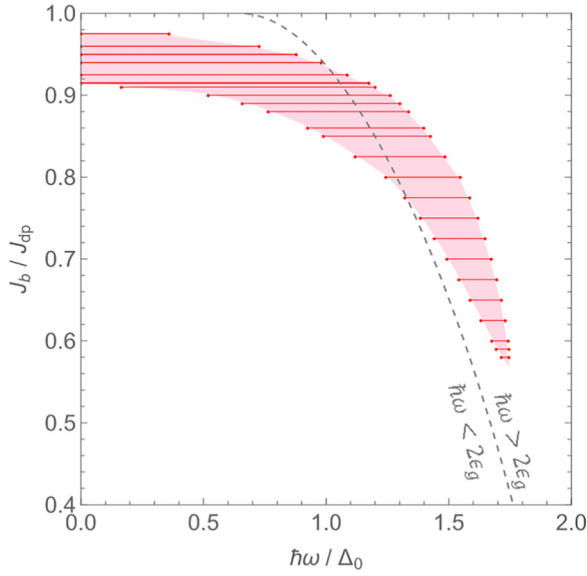
FIG. 6. The Higgs-induced instability domain in the ω-J_b plane for the ac $\parallel$ dc configuration. The colored region represents the parameter space in which $\operatorname{Im}\sigma(J_b,\omega)<0$, indicating that the homogeneous current-carrying state is unstable against ac perturbations. Within this instability region, the system may transition into an inhomogeneous state, leading to phase slips or vortex nucleation. For comparison, the dashed curve represents the spectral gap $2\epsilon_g(J_b)$.

is entirely absent in the ac $\perp$ dc configuration. Further discussion on this topic is provided in Sec. V B.

In the next section, we focus on bias-dependent kinetic inductance, a key quantity in superconducting-device applications. While the primary emphasis is on the kinetic inductance, the Higgs-induced instability plays a crucial role in its behavior. Thus, we revisit this instability within the kinetic inductance framework, offering a more intuitive perspective that enhances comprehension.

IV. BIAS-DEPENDENT KINETIC INDUCTANCE

A. Kinetic inductivity

The kinetic inductivity is defined by $L_k \dot{J}_s = E$ or, equivalently, in the frequency domain, $L_k\{-i\omega J_s(\omega)\} = E(\omega)$. Here, the reactive component of the current density is given by $J_s = i\sigma_2 E$ and $\sigma_2 := \operatorname{Im}\sigma$. Thus, the kinetic inductivity can be expressed as

$$L_k = \frac{1}{\omega\sigma_2} \tag{45}$$

$$= \begin{cases} \left\{\omega(\sigma_2^{(0)} + \sigma_2^{(1)} + \sigma_2^{(2)})\right\}^{-1} & (\text{ac} \parallel \text{dc}), \\ \left(\omega\sigma_2^{(0)}\right)^{-1} & (\text{ac} \perp \text{dc}). \end{cases} \tag{46}$$

Here, $\sigma_2^{(i)} := \operatorname{Im}\sigma^{(i)}$ ($i=0,1,2$). For example, in the zero-bias ($s=0$), low-frequency ($\hbar\omega \ll \Delta_0$), and low-temperature ($kT \ll \Delta_0$) limit, translating the integral over ϵ into a Matsubara summation yields $\sigma_{20} := \sigma_2(0,0,0) = \sigma_2^{(0)}(0,0,0) = 1/\mu_0\omega\lambda_0^2 = \pi\Delta_0\sigma_n/\hbar\omega$, reproducing the well-known result $L_{k0} = 1/\omega\sigma_{20} = \mu_0\lambda_0^2$.

B. Behavior in the small-bias regime

While our formulation applies to arbitrary bias dc strengths, particular insight can be gained by examining the small-bias regime ($J_b \ll J_{dp}$). In this regime, the kinetic inductance follows Eq. (1), where the coefficient C plays a crucial role in distinguishing between the oscillating and frozen superfluid density regimes. As we will demonstrate later in this subsection, these regimes correspond to the ac $\parallel$ dc and ac $\perp$ dc configurations, respectively.

Evaluating C is straightforward. Using Eq. (45), we can rewrite

$$\frac{L_k(J_b)}{L_k(0)} = 1 + C\left(\frac{J_b}{J_{dp}}\right)^2 \tag{47}$$

as

$$\frac{\sigma_2(J_b)}{\sigma_2(0)} = 1 - C\left(\frac{J_b}{J_{dp}}\right)^2, \tag{48}$$

which is valid in the small-bias regime. By calculating σ_2 and incorporating the effects of the bias dc up to order $s/\Delta_0 \sim (J_b/J_{dp})^2$, we can determine the coefficient C.

We begin by focusing on the low-frequency ($\hbar\omega \ll \Delta$) and low-temperature ($T \ll T_c$) regime. This focus is motivated by two key reasons. First, in this regime, the coefficient C can be calculated analytically. Second, many superconducting materials used in practical devices operate at technologically relevant frequencies (approximately gigahertz), which generally satisfy $\hbar\omega \ll \Delta_0$, and their operating temperatures are typically in the low-temperature limit ($T \ll T_c$). Thus, the low-frequency and low-temperature regime is of both theoretical and practical importance.

The calculation of $\sigma_2^{(0)} := \operatorname{Im}\sigma^{(0)}$ proceeds as follows. In the low-frequency limit, $\sigma_2^{(0)}$, given by Eq. (41), reduces to the Matsubara sum $(4\pi kT\sigma_n/\hbar\omega)\sum_{\omega_m>0}F_m^2$. Using Eq. (23), this evaluates to $1/\mu_0\omega\lambda^2(s,T)$ for any bias and temperature. For $T \to 0$, the Matsubara summation $2\pi kT\sum_{\omega_m>0}(\dots)$ can be replaced by the integral $\Delta_0\int_0^\infty(\dots)dw$, where $w = \hbar\omega_m/\Delta_0$. Performing this substitution yields

$$\left.\frac{\sigma_2^{(0)}(s,\omega,T)}{\sigma_{20}}\right|_{\omega\ll\frac{\Delta_0}{\hbar},\,T\ll T_c} = 1 - \left(\frac{\pi}{4} + \frac{4}{3\pi}\right)\frac{s}{\Delta_0} + \mathcal{O}(s^2). \tag{49}$$

The calculations of $\sigma_2^{(1,2)} := \operatorname{Im}\sigma^{(1,2)}$ are more straightforward. Since this subsection considers the effects of the bias dc up to the order of $\mathcal{O}(s)$, we can substitute the zero-current Green's functions in place of G_b and F_b in Eqs. (42) and (43), leading to

$$\left.\frac{\sigma_2^{(1)}(s,\omega,T)}{\sigma_{20}}\right|_{\omega\ll\frac{\Delta_0}{\hbar},\,T\ll T_c} = -\frac{8}{3\pi}\frac{s}{\Delta_0} + \mathcal{O}(s^2), \quad (50)$$

$$\left.\frac{\sigma_2^{(2)}(s,\omega,T)}{\sigma_{20}}\right|_{\omega\ll\frac{\Delta_0}{\hbar},\,T\ll T_c} = \Psi\frac{s}{\Delta_0} + \mathcal{O}(s^2). \quad (51)$$

Here, Ψ for $\hbar\omega \ll \Delta_0$ can also be evaluated analytically in a similar manner. In the numerator, the integral simplifies to -2π as $T \to 0$. For the denominator, the integral simplifies to $4(\sinh^{-1}\tilde{\omega}_c - 1)$, where $\tilde{\omega}_c = \hbar\omega_c/\Delta_0$ is the dimensionless cutoff energy of the Matsubara sum, with ω_c typically set near the Debye frequency. The BCS coupling constant $\mathcal{G}$ can be eliminated by utilizing the BCS relation $1 = \mathcal{G}\sinh^{-1}\tilde{\omega}_c$, yielding

$$\Psi(s,\omega,T)|_{\omega\ll\frac{\Delta_0}{\hbar},\,T\ll T_c} = -\frac{\pi}{2}. \quad (52)$$

The next step is to express s/Δ_0 in terms of J_b/J_{dp}. In general, as illustrated in Fig. 2(a), J_b/J_{dp} exhibits a nonlinear dependence on $s/\Delta_0 = (q_b/q_\xi)^2$. However, in the small-bias regime ($J_b/J_{dp} \ll 1$), this relationship simplifies to a linear form, $J_b/J_{dp} = kq_b/q_\xi$, which leads to $s/\Delta_0 = k^{-2}(J_b/J_{dp})^2$. While the slope $k(T)$ generally needs to be determined numerically for a given temperature T, its analytical expression at $T \to 0$ is derived in Appendix A as

$$k(0) = \frac{1}{\sqrt{s_d/\Delta_0}\,(\Delta_d/\Delta_0 - 4s_d/3\pi\Delta_0)} \simeq 2.98. \quad (53)$$

Here, $\eta_d = 2\pi + 3\pi/8 - \sqrt{(2/\pi + 3\pi/8)^2 - 1} = 0.300$, $\Delta_d/\Delta_0 = e^{-\pi\eta_d/4} = 0.790$, and $s_d/\Delta_0 = \eta_d(\Delta_d/\Delta_0) = 0.237$.

Finally, we arrive at the analytical expression for C in the low-frequency and low-temperature regime. The result is

$$C = \begin{cases} C^{(0)} + C^{(1)} + C^{(2)} & (\text{ac}\parallel\text{dc}) \\ C^{(0)} & (\text{ac}\perp\text{dc}) \end{cases}$$

$$\simeq \begin{cases} 0.409 & (\text{ac}\parallel\text{dc}) \\ 0.136 & (\text{ac}\perp\text{dc}). \end{cases} \quad (54)$$

Here, the contributions are

$$C^{(0)} = \left(\frac{\pi}{4} + \frac{4}{3\pi}\right)\frac{s_d}{\Delta_0}\left(\frac{\Delta_d}{\Delta_0} - \frac{4s_d}{3\pi\Delta_0}\right)^2 \simeq 0.136, \quad (55)$$

$$C^{(1)} = \frac{8}{3\pi}\frac{s_d}{\Delta_0}\left(\frac{\Delta_d}{\Delta_0} - \frac{4s_d}{3\pi\Delta_0}\right)^2 \simeq 0.0956, \quad (56)$$

$$C^{(2)} = \frac{\pi}{2}\frac{s_d}{\Delta_0}\left(\frac{\Delta_d}{\Delta_0} - \frac{4s_d}{3\pi\Delta_0}\right)^2 \simeq 0.177. \quad (57)$$

It follows that $C^{(1)} + C^{(2)} = 2C^{(0)}$. The above results indicate that more than 40% of the bias dependence in the ac $\parallel$ dc configuration originates from the contribution of the Higgs mode.

The resulting values of C for the ac $\parallel$ dc and ac $\perp$ dc configurations precisely match the previous calculations based on the thermodynamic Usadel equation combined with the oscillating and frozen superfluid density assumptions, respectively [24,25]. Notably, while a prior study by the author [10] has identified these coincidences through numerical calculations based on the Keldysh-Eilenberger equation, we now confirm them analytically.

It should be noted that the above coefficient C is evaluated in the dirty limit at $T = 0$. For different mean free paths and temperatures, C varies, and its numerical evaluation can be found in Ref. [10].

C. Kinetic inductance under arbitrary bias strength and Higgs-induced instability

The calculation of bias-dependent L_k for an arbitrary bias dc strength [see Eq. (45)] follows the same procedure as the evaluation of $\operatorname{Im}\sigma$ presented in Figs. 4–6.

In Fig. 7(a), we illustrate the frequency dependence of $L_k(\omega)$ for small to moderately strong bias dc values in the ac $\parallel$ dc configuration. In this regime, $L_k(\omega)$ exhibits weak frequency dependence, except around $\hbar\omega \simeq 2\Delta$, where a pronounced peak emerges due to the Higgs-mode contribution. This peak directly corresponds to the dip observed in $\operatorname{Im}\sigma$ [see Fig. 5(e)]. It is worth noting that, in the ac $\perp$ dc configuration, the Higgs-induced peak vanishes, resulting in $L_k(\omega)$ exhibiting a monotonically increasing trend with weak frequency dependence [see also Fig. 4].

As the bias dc strength increases further ($J_b/J_{dp} \gtrsim 0.6$), as shown in Fig. 7(b), the peak in L_k diverges at the characteristic frequencies ω_1 and ω_2, where $\operatorname{Im}\sigma = 0$. The frequency range $\omega_1 < \omega < \omega_2$, where $L_k < 0$, marks the onset of Higgs-induced instability in the homogeneous current-carrying state under ac perturbations, potentially leading to phase slips or vortex nucleation (see also the discussion in Sec. III B).

With further increase in the bias strength [see Fig. 7(c)], the instability window shifts to lower frequencies, eventually reaching $\omega_1 \to 0$, where the instability domain spans the range $0 < \omega < \omega_2$.
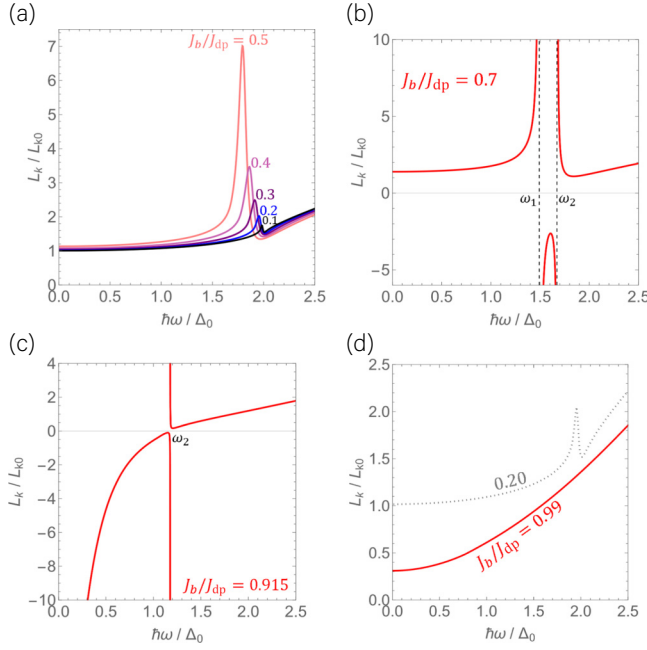
FIG. 7. The frequency dependence of the kinetic inductance L_k at $T = 0$ for the ac $\parallel$ dc configuration, calculated at various dc biases: (a) $J_b/J_{dp} = 0.1$–0.5, (b) $J_b/J_{dp} = 0.7$, (c) $J_b/J_{dp} = 0.915$, and (d) $J_b/J_{dp} = 0.99$. The occurrence of negative L_k indicates the instability of the homogeneous current-carrying state, leading to a transition into an inhomogeneous state, such as phase slips or vortex nucleation. It is important to note that in real experiments, rather than directly observing negative values, L_k corresponding to these inhomogeneous states is expected to be measured, along with a finite voltage generated by moving vortices.

For even stronger dc bias [see Fig. 7(d)], ω_2 also shifts toward zero. At this stage, the homogeneous current-carrying state regains stability across the entire ac spectrum. Interestingly, the kinetic inductance in this regime is found to be smaller than that in the zero-current state.

For completeness, we summarize the above findings in terms of bias dependence. In Fig. 8(a), we present $L_k(J_b)$ for a low-frequency ac perturbation ($\hbar\omega/\Delta_0 = 0.01$). As the dc bias increases, L_k initially rises and diverges to $+\infty$, before abruptly dropping to negative values around $J_b/J_{dp} \simeq 0.9$, signaling the Higgs-induced instability of the homogeneous current-carrying state (see the left edge of Fig. 6). For $J_b/J_{dp} \gtrsim 0.98$, stability is restored and L_k regains positive values. Interestingly, in this regime, L_k is smaller than that of the zero-current state. It is important to note that a negative L_k signifies instability rather than a physically observable quantity. In real experiments, instead of directly measuring negative L_k, one would observe an effective L_k corresponding to the emergent inhomogeneous states, which include vortices and are accompanied by a finite voltage due to vortex motion.

In Fig. 8(b), we present $L_k(J_b)$ for an ac perturbation with frequency $\hbar\omega/\Delta_0 = 1.75$. In this case, no negative
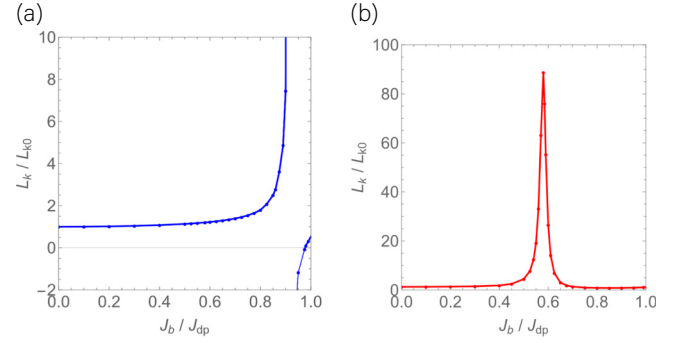

FIG. 8. The bias dc dependence of the kinetic inductance L_k for the ac $\parallel$ dc configuration, calculated at $T = 0$. The frequency of the ac perturbation is (a) $\hbar\omega/\Delta_0 = 0.01$ and (b) $\hbar\omega/\Delta_0 = 1.75$. Negative L_k signals the instability of the homogeneous current-carrying state, leading to a transition into an inhomogeneous state with phase slips or vortex nucleation. In real experiments, rather than observing negative values, an effective L_k associated with these inhomogeneous states is expected to be measured.

$L_k(J_b)$ appears, confirming the absence of instability (see also the corresponding frequency in Fig. 6). Instead, a pronounced peak emerges, associated with a tiny $\text{Im}\,\sigma$ at the boundary of the instability domain. The maximum value of L_k occurs around half the depairing current and is nearly 2 orders of magnitude larger than its zero-current counterpart.

V. DISCUSSION AND CONCLUSIONS

In this paper, we have investigated a dirty-limit superconductor subjected to a perturbative ac field superposed on a dc bias of arbitrary strength. Our analysis has revealed that strong dc biases parallel to the ac field give rise to highly nontrivial effects due to the pronounced contribution of the Higgs mode in dirty superconductors, leading to striking phenomena that cannot be captured in the weak-bias regime. Below, we summarize our key findings and discuss their implications for applied superconductivity.

A. Complex-conductivity formula

In Sec. II, we have derived the complex-conductivity formula for a disordered superconductor subjected to an ac perturbation superposed on a dc bias of arbitrary strength using the Keldysh-Usadel theory of nonequilibrium superconductivity. This formula, given by Eq. (40), represents one of the main results of this paper. In the weak-dc-bias regime, where the bias can be treated as a perturbation, our formula reproduces the results obtained by Moor *et al.* [7]. Furthermore, it serves as the dirty-limit counterpart of the more general expression derived from the Keldysh-Eilenberger theory in Refs. [9,10].

It is important to note that previous studies investigating the ac response under a strong dc bias in

the context of superconducting-device applications (see, e.g., Refs. [27,40–42]) have considered only the contribution from Eq. (41) while neglecting the additional contributions from Eqs. (42) and (43). However, their results remain valid within the specific context of the ac ⊥ dc configuration, where the Higgs mode is not excited.

For instance, in Refs. [40,41] it was demonstrated that Reσ exhibits a dc-bias-dependent reduction at low frequencies and at moderately low temperatures, suggesting the possibility of tuning dissipation via the bias dc. These findings hold for the ac ⊥ dc configuration, where the Higgs mode is not excited. In contrast, for the ac ∥ dc configuration, the additional contributions from Eqs. (42) and (43) significantly modify Reσ, as shown in Ref. [10]. This results in a dc-bias-dependent suppression of Reσ that extends to higher bias strengths and higher frequencies.

We treat a diffusive superconductor that carries a dc superflow and is perturbed by a weak ac field within the nonequilibrium Keldysh-Usadel framework. Three other impurity-based approaches are available, i.e., nonlinear Mattis-Bardeen (MB) theory [20], the self-consistent Born approximation (SCBA) [21], and real-space time-dependent Bogoliubov–de Gennes (td-BdG) calculations [22], but they have been worked out only for zero-bias or purely ac driving. The MB extension and the SCBA-Eilenberger-Usadel hierarchy share the same Born impurity ladder: a Fermi-surface average takes SCBA to the homogeneous Eilenberger equation, which becomes Usadel in the diffusive limit, and the nonlinear MB calculation yields the same third-order conductivity as obtained by Eilenberger expansion [19]. The td-BdG simulation treats disorder nonperturbatively; in the weak-disorder regime it nevertheless converges to the same third-harmonic response and, beyond that regime, captures strong-disorder effects that are inaccessible to Born-level theories. Recasting any of these formalisms for the combined dc+ac drive considered here is therefore expected to yield the same conductivity in the common-parameter window of weak, isotropic disorder, while differences would arise only outside that range.

B. Higgs-induced instability of the homogeneous current-carrying state

In Sec. III, we have demonstrated the Higgs-induced instability of the homogeneous current-carrying state, which arises in the ac ∥ dc configuration under a strong dc bias. As the bias increases beyond $J_b/J_{dp} \gtrsim 0.6$, the Higgs-mode contribution to Imσ becomes strongly negative within a certain frequency range, leading to the emergence of a window in which Im$\sigma < 0$, indicating a negative kinetic inductance $(\omega\mathrm{Im}\,\sigma)^{-1} < 0$. This negative kinetic inductance implies that the kinetic energy

decreases with increasing current, rendering the homogeneous current-carrying state unstable. Accordingly, our ansatz of a homogeneous solution becomes invalid within the regime in which Imσ is negative and the system is expected to transition into an inhomogeneous state through vortex nucleation. This instability is mapped in the ω-J_b plane in Fig. 6.

It should be noted that this instability map is specific to the dirty limit. As the mean free path increases, the Higgs-mode contribution to Imσ is suppressed [10], shifting the instability window to higher bias currents until it eventually disappears at a critical mean free path. Determining this critical mean free path is feasible using the theoretical framework developed in Refs. [9,10], presenting an interesting direction for future research.

In the present paper, the damping factor is fixed at $\Gamma/\Delta_0 = 10^{-5}$, which is extremely small and has negligible influence on the calculated results for σ. Nonetheless, the impact of a moderately large Γ on σ has attracted interest in the superconducting-device community (see, e.g., Refs. [24,38] and references therein). A preliminary comparison presented in Appendix D shows that increasing Γ slightly shifts the peak and dip positions in both Reσ and Imσ to lower frequencies. A more detailed and systematic investigation of the effects of finite Γ on σ and the associated instability lies beyond the scope of this paper but represents an important direction for future research.

The author recently became aware of Ref. [39], in which a model is investigated where the Higgs mode is excited through modulation of the BCS coupling. The authors' study shows that the homogeneous solution can lead to a negative superfluid density, signaling an instability, and that phase slips begin to proliferate once the superfluid density becomes negative. In our work, the Higgs mode is excited by an ac perturbation superposed on a strong dc bias, whereas in their model, it is driven by BCS coupling modulation. Despite these different excitation mechanisms, both studies highlight the critical role of the Higgs mode in destabilizing the homogeneous superconducting state. Additionally, it is reported in Ref. [43] that in the dirty limit, the Higgs contribution can lead to negative Imσ, in agreement with our findings. A more detailed and systematic theoretical investigation of this phenomenon is necessary. Although beyond the scope of this paper, it remains an important challenge for future research.

A potential experimental verification of this instability could be achieved by measuring the voltage along a dc-biased superconducting wire under ac illumination. When the combination of ac frequency and bias current falls within the instability region shown in Fig. 6, the homogeneous current-carrying state transitions into an inhomogeneous state via vortex nucleation, generating a finite voltage due to vortex motion. It is important to note that if the ac perturbation frequency exceeds the spectral gap ($\hbar\omega > 2\epsilon_g$), quasiparticle-induced dissipation may

significantly increase the temperature of the superconducting wire, potentially interfering with the measurement. To mitigate this effect, it is preferable to focus on lower frequencies, which correspond to the region on the left side of the dashed curve in Fig. 6. This ensures that the instability dynamics remain dominated by the Higgs mode rather than excessive quasiparticle excitations.

C. Kinetic inductance under a weak dc bias

In Sec. IV B, we have investigated the bias-dependent kinetic inductance for $J_b \ll J_{dp}$, a key parameter for superconducting-device applications. For small dc biases, L_k follows the small-bias expansion in Eq. (1), increasing monotonically with J_b. The coefficient C for the ac $\parallel$ dc ($C \simeq 0.409$) and ac $\perp$ dc ($C \simeq 0.136$) configurations exactly matches previous results for dirty-limit superconductors, corresponding to the oscillating and frozen superfluid density assumptions, respectively [24,25]. While this agreement was previously confirmed numerically in Ref. [10] using the Keldysh-Eilenberger theory, our results now provide an analytical verification.

The oscillating and frozen superfluid density assumptions were originally termed *slow* and *fast* experiment assumptions, based on whether the ac frequency is below or above the inverse relaxation time of n_s. However, Ref. [10] and this work clarify that the true distinction arises not from ac frequency but from Higgs-mode excitation: active in ac $\parallel$ dc and absent in ac $\perp$ dc.

To experimentally determine the coefficient C and validate the theory, one can employ techniques such as those described in Refs. [44–50]. It is important to note that the value of C obtained in this paper is strictly valid for the dirty limit. For arbitrary mean free paths, C can be computed using the Keldysh-Eilenberger theory, as shown in Ref. [10, Fig. 8(d)].

D. Kinetic inductance under a dc bias approaching J_{dp}

In Sec. IV C, we have examined the impact of stronger dc biases on L_k. It has been shown that the Higgs-induced instability leads to a divergence in L_k, followed by an abrupt drop to negative values [see Fig. 8(a)]. This negative L_k signifies a transition to an inhomogeneous state, typically involving phase slips or vortex dynamics. In real experiments, rather than directly observing negative L_k, one would measure an effective L_k corresponding to these emergent inhomogeneous states. Since our analysis is based on the homogeneous current-carrying solution, it does not apply to calculating L_k within the inhomogeneous regime. What we can conclude is that L_k diverges and then takes a finite value close to J_{dp}, which is consistent with the experimentally observed suppression of kinetic inductance near the depairing current [44,45]. A detailed investigation of the inhomogeneous state would provide a quantitative explanation for this phenomenon. Although this is beyond

the scope of this paper, it remains an important challenge for future research.

Interestingly, by exploiting the L_k divergence at the boundary of the instability domain (see Fig. 6), kinetic inductance can be significantly enhanced. For instance, in Fig. 8(b) it is shown that L_k can exceed the zero-current value by nearly 2 orders of magnitude, well below J_{dp}. These findings indicate that by carefully tuning the bias strength and ac frequency, the Higgs mode can be utilized to control and optimize kinetic inductance in superconducting devices.

E. Other implications for superconducting-device applications

The Higgs-induced instability renders a homogeneous high-current-carrying state susceptible to bias fluctuations or stray subgap photons, such as black-body radiation, when (ω, J_b) falls within the instability domain shown in Fig. 6. This can lead to a transition into an inhomogeneous state via vortex nucleation. It is possible that this effect has already manifested in various superconducting applications without being explicitly recognized.

In superconducting nanowire and microstrip single-photon detectors, achieving a low dark-count rate (DCR) is crucial for high-performance photon detection. Several known mechanisms contribute to DCR, including black-body radiation [4], vortex crossings due to current-assisted unbinding of vortex-antivortex pairs [51], and thermal fluctuations [52]. While current technology has significantly reduced DCR, further studies are necessary to fully identify and mitigate the remaining sources of dark counts. Since these photon detectors operate under a strong dc bias close to J_{dp}, ac perturbations falling within the Higgs-induced instability domain shown in Fig. 6 may contribute to DCR. This potential contribution of Higgs-mode-induced instability to DCR has not been considered in previous studies and could be an overlooked factor in understanding its origins.

The ultimate accelerating gradient of superconducting cavities for particle accelerators is believed to be limited by the superheating field B_{sh} [24,53–59], which represents the stability threshold of the Meissner state and corresponds to the magnetic field at which the surface current density reaches J_{dp}. Since the Higgs-induced instability weakens the stability of the current-carrying state near J_{dp}, it is natural to expect that the dc superheating field is also susceptible to ac perturbations. The onset of instability under an ac perturbation occurs at $J_b/J_{dp} \gtrsim 0.6$, suggesting that the dirty-limit superheating field [24,55,58], $B_{sh} \simeq 0.8 B_c$, may become unstable against ac perturbations at approximately $B \sim 0.6 \times 0.8 B_c \simeq 0.4 B_c < B_{sh}$. However, it should be noted that in clean superconductors, the Higgs mode is significantly weaker, implying that the Higgs-induced instability may not be relevant in that regime.

A superconducting diode exhibits an asymmetric critical current, allowing dissipationless current flow in one direction while suppressing it in the opposite direction. The system considered in this paper is particularly relevant to superconducting diodes based on simple conventional superconductors (see, e.g., Refs. [60–63]). If one polarity of the critical current falls within the instability domain, the homogeneous current-carrying state in this direction may become unstable against ac perturbations, potentially degrading the performance of the superconducting diode. This suggests that the Higgs-induced instability could be an overlooked factor influencing the robustness and efficiency of superconducting diodes under strong dc bias.

This instability is expected to be a ubiquitous phenomenon in superconducting applications that employ disordered superconductors under strong dc bias. To mitigate this instability, the most straightforward approach is to increase the mean free path of the material, which suppresses the Higgs-resonance dip in $\text{Im}\,\sigma$ (see Refs. [9,10]) and effectively raises the instability threshold to higher bias currents.

Conversely, this instability could be exploited to design a new class of superconducting detectors. Since the instability frequency window depends on the dc-bias strength (see Fig. 6), the sensitive frequency range can be dynamically tuned via the applied bias.

DATA AVAILABILITY

The numerical data used to generate the figure plots are openly available [64]; embargo periods may apply.

APPENDIX A: SOLUTION OF THE THERMODYNAMIC USADEL EQUATION AT $T \to 0$

In this appendix, we summarize the known solution for $T \to 0$, originally derived by Maki several decades ago [31,32]:

$$\frac{\Delta_b(s,0)}{\Delta_0} = \exp\left[-\frac{\pi s}{4\Delta_b(s,0)}\right], \qquad (A1)$$

$$\frac{n_s(s,0)}{n_{s0}} = \frac{\lambda_0^2}{\lambda^2(s,0)} = \frac{\Delta_b(s,0)}{\Delta_0} - \frac{4s}{3\pi\Delta_0}, \qquad (A2)$$

$$J_b(s,0) = \sqrt{\frac{\pi s}{\Delta_0}}\left\{\frac{\Delta_b(s,0)}{\Delta_0} - \frac{4s}{3\pi\Delta_0}\right\}\frac{H_{c0}}{\lambda_0}. \qquad (A3)$$

The depairing current density at $T = 0$, corresponding to the maximum value of $J_b(s,0)$, is given by

$$J_{dp}(0) = \sqrt{\frac{\pi s_d}{\Delta_0}}\left\{\frac{\Delta_d}{\Delta_0} - \frac{4s_d}{3\pi\Delta_0}\right\}\frac{H_{c0}}{\lambda_0} = 0.595\frac{H_{c0}}{\lambda_0}, \quad (A4)$$

$$\eta_d = \frac{2}{\pi} + \frac{3\pi}{8} - \sqrt{\left(\frac{2}{\pi} + \frac{3\pi}{8}\right)^2 - 1} = 0.300, \qquad (A5)$$

$$\Delta_d/\Delta_0 = e^{-\pi\eta_d/4} = 0.790, \qquad (A6)$$

$$s_d/\Delta_0 = \eta_d\Delta_d/\Delta_0 = 0.237. \qquad (A7)$$

In particular, for a small-bias dc, the superconducting gap behaves as $\Delta(s)/\Delta_0 = 1 - \pi s/4\Delta_0$ and the current density follows $J_b(s,0) = \sqrt{\pi s/\Delta_0}H_{c0}/\lambda_0$. This leads to the relation

$$s = s_d\left(\frac{\Delta_d}{\Delta_0} - \frac{4s_d}{3\pi\Delta_0}\right)^2\left(\frac{J_b}{J_{dp}}\right)^2 \qquad (A8)$$

for $T \to 0$ and $s/\Delta_0 \ll 1$, which is useful for converting s into J_b in the small bias dc regime.

APPENDIX B: SANITY CHECK: REPRODUCING THE RESULTS OF MOOR *et al.*

Our formulation and results apply to arbitrary bias dc strengths. However, as a consistency check, it is useful to consider the perturbative bias dc limit. This case was analyzed in the pioneering work of Moor *et al.* [7], where both the ac field and dc bias were treated as perturbations.

In this limit, we can use the zero-current Green functions $G_0 = (\epsilon + i0)/\sqrt{(\epsilon + i0)^2 - \Delta^2}$ and $F_0 = \Delta/\sqrt{(\epsilon + i0)^2 - \Delta^2}$. Substituting G_0 and F_0 into G_b and F_b in Eqs. (29), (30), (34), and (35), we obtain

$$\zeta = \frac{G_{0+}G_{0-} + F_{0+}F_{0-} + 1}{\sqrt{+} + \sqrt{-}}, \qquad (B1)$$

$$\zeta^a = \frac{-G_{0+}G_{0-}^* - F_{0+}F_{0-}^* + 1}{\sqrt{+} - \sqrt{-}^*}, \qquad (B2)$$

$$\kappa = -i\frac{2\epsilon\Delta(G_{0+} + G_{0-})}{\sqrt{+}\sqrt{-}\left(\sqrt{+} + \sqrt{-}\right)}, \qquad (B3)$$

$$\kappa^a = i\frac{2\epsilon\Delta(G_{0+} - G_{0-}^*)}{\sqrt{+}\sqrt{-}^*\left(\sqrt{+} - \sqrt{-}^*\right)}, \qquad (B4)$$

where $\sqrt{\pm} := \sqrt{(\epsilon + i0 \pm \hbar\omega/2)^2 - \Delta^2}$.

These expressions exactly reproduce the results obtained by Moor *et al.* [7]. Furthermore, the same results can be derived from the leading-order approximation of the Keldysh-Eilenberger theory in the dirty limit [10]. This provides additional validation of our approach.

APPENDIX C: RELATIVE CONTRIBUTIONS OF $\sigma^{(0)}$, $\sigma^{(1)}$, AND $\sigma^{(2)}$ TO THE COMPLEX CONDUCTIVITY

To clarify the relative magnitude and physical origin of each component of the complex conductivity, we explicitly compare the individual contributions of $\sigma^{(0)}$, $\sigma^{(1)}$, and $\sigma^{(2)}$, as introduced in Eq. (40). These three components originate from distinct mechanisms. $\sigma^{(0)}$ is a natural extension of the Mattis-Bardeen conductivity from the zero-bias case to finite dc bias, obtained by replacing the zero-current Green's functions with G_b and F_b, which represent the equilibrium solutions in the presence of a dc bias. In contrast, $\sigma^{(1)}$ and $\sigma^{(2)}$ arise from the Doppler fluctuation of the superflow, $\delta W \propto \mathbf{q}_b \cdot \delta \mathbf{q}_\omega$, which drives the nonequilibrium corrections to the Green's functions [see Eqs. (27)–(39)]. Among these, the terms proportional to the Higgs-mode amplitude Ψ constitute the Higgs-mode contribution $\sigma^{(2)}$.

In Fig. 9, we present a representative comparison of $\mathrm{Re}\,\sigma^{(0,1,2)}$ and $\mathrm{Im}\,\sigma^{(0,1,2)}$ as functions of frequency, evaluated at fixed dc biases $J_b/J_{\mathrm{dp}} = 0.55$ and 0.925 and temperature $T = 0$, for the ac $\parallel$ dc configuration.

For the real part, near the gap edge $\hbar\omega \simeq 2\epsilon_g(J_b)$, both $\sigma^{(0)}$ and $\sigma^{(1)}$ begin to increase. However, the Higgs-mode contribution $\sigma^{(2)}$ becomes significantly larger than either of them and dominates the overall conductivity in this frequency range.

FIG. 10. A comparison of the complex conductivity σ at $T = 0$ and $J_b/J_{\mathrm{dp}}(\Gamma) = 0.65$ for two different damping factors—the small value $\Gamma/\Delta_0 = 10^{-5}$ used throughout this study and a moderately larger value $\Gamma/\Delta_0 = 0.02$—for the ac $\parallel$ dc configuration. (a),(b) The (a) real and (b) imaginary parts of σ as functions of frequency.

For the imaginary part, below the gap edge $\hbar\omega \simeq 2\epsilon_g(J_b)$, the Doppler-fluctuation contributions $\sigma^{(1)}$ and $\sigma^{(2)}$ are both negative. When the dc bias is moderately strong, $\sigma^{(0)}$ dominates the total conductivity and maintains $\mathrm{Im}\,\sigma$ positive, resulting in only a small dip. However, under sufficiently strong dc bias, the Higgs-mode contribution $\sigma^{(2)}$ becomes large enough to drive $\mathrm{Im}\,\sigma$ negative over a finite frequency range, indicating the onset of the Higgs-induced instability.

APPENDIX D: IMPACT OF A MODERATELY LARGE DAMPING FACTOR

In the present paper, the damping factor is fixed at $\Gamma/\Delta_0 = 10^{-5}$, which is extremely small and does not significantly affect the calculated results for σ. Understanding how increasing Γ/Δ_0 influences σ and the associated Higgs-induced instability is an interesting and important question for future investigation.

As a preliminary comparison, we evaluate σ at $J_b/J_{\mathrm{dp}}(\Gamma) = 0.65$ for both the small damping factor $\Gamma/\Delta_0 = 10^{-5}$ used throughout the main text and a moderately larger value $\Gamma/\Delta_0 = 0.02$. Note that J_{dp} depends on Γ, as discussed in Refs. [24,38]. As expected, increasing Γ slightly shifts the peak and dip structures in both $\mathrm{Re}\,\sigma$ and $\mathrm{Im}\,\sigma$ to lower frequencies, due to the suppression of superconductivity induced by the larger damping.

A more detailed and systematic investigation of the effects of finite Γ on the Higgs-induced instability lies beyond the scope of this paper, but would be a worthwhile direction for future research.
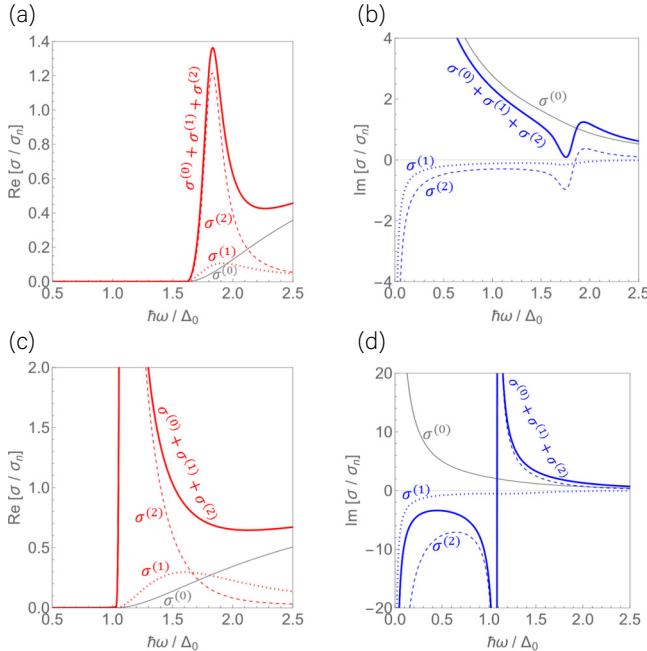

FIG. 9. The relative contributions of $\sigma^{(0)}$, $\sigma^{(1)}$, and $\sigma^{(2)}$ to the total complex conductivity $\sigma = \sigma^{(0)} + \sigma^{(1)} + \sigma^{(2)}$ at temperature $T = 0$ in the ac $\parallel$ dc configuration. (a),(b) The real and imaginary parts, respectively, for $J_b/J_{\mathrm{dp}} = 0.55$. (c),(d) The corresponding results for $J_b/J_{\mathrm{dp}} = 0.925$.
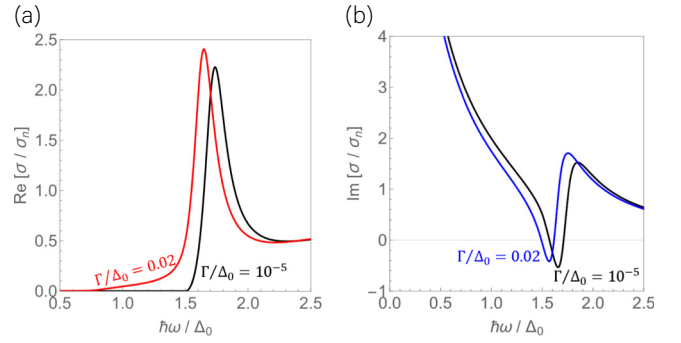
[1] J. Zmuidzinas, Superconducting microresonators: Physics and applications, Annu. Rev. Condens. Matter Phys. **3**, 169 (2012).

[2] M. R. Vissers, R. P. Erickson, H.-S. Ku, L. Vale, X. Wu, G. C. Hilton, and D. P. Pappas, Low-noise kinetic inductance traveling-wave amplifier using three-wave mixing, Appl. Phys. Lett. **108,** 012601 (2016).

[3] H. Shishido, S. Miyajima, Y. Narukami, K. Oikawa, M. Harada, T. Oku, M. Arai, M. Hidaka, A. Fujimaki, and T. Ishida, Neutron detection using a current biased kinetic inductance detector, Appl. Phys. Lett. **107,** 232601 (2015).

[4] I. E. Zadeh, J. Chang, J. W. N. Los, S. Gyger, A. W. Elshaari, S. Steinhauer, S. N. Dorenbos, and V. Zwiller, Superconducting nanowire single-photon detectors: A perspective on evolution, state-of-the-art, future developments, and applications, Appl. Phys. Lett. **118,** 190502 (2021).

[5] F. Ando, Y. Miyasaka, T. Li, J. Ishizuka, T. Arakawa, Y. Shiota, T. Moriyama, Y. Yanase, and T. Ono, Observation of superconducting diode effect, Nature **584,** 373 (2020).

[6] A. Gurevich, Theory of RF superconductivity for resonant cavities, Supercond. Sci. Technol. **30,** 034004 (2017).

[7] A. Moor, A. F. Volkov, and K. B. Efetov, Amplitude Higgs mode and admittance in superconductors with a moving condensate, Phys. Rev. Lett. **118,** 047001 (2017).

[8] S. Nakamura, Y. Iida, Y. Murotani, R. Matsunaga, H. Terai, and R. Shimano, Infrared activation of the Higgs mode by supercurrent injection in superconducting NbN, Phys. Rev. Lett. **122,** 257001 (2019).

[9] T. Jujo, Surface resistance and amplitude mode under uniform and static external field in conventional superconductors, J. Phys. Soc. Jpn. **91,** 074711 (2022).

[10] T. Kubo, Significant contributions of the Higgs mode and impurity-scattering self-energy corrections to the low-frequency complex conductivity in dc-biased superconducting devices, Phys. Rev. Appl. **22,** 044042 (2024).

[11] P. W. Anderson, Random-phase approximation in the theory of superconductivity, Phys. Rev. **112,** 1900 (1958).

[12] A. F. Volkov and S. M. Kogan, Collisionless relaxation of the energy gap in superconductors, Sov. J. Exp. Theor. Phys. **38,** 1018 (1974).

[13] R. Shimano and N. Tsuji, Higgs mode in superconductors, Annu. Rev. Condens. Matter Phys. **11,** 103 (2020).

[14] N. Tsuji, I. Danshita, and S. Tsuchiya, in *Encyclopedia of Condensed Matter Physics*, edited by T. Chakraborty (Academic Press, Canmbridge, Massachusetts, 2024), 2nd ed., p. 174.

[15] R. Matsunaga, Y. I. Hamada, K. Makise, Y. Uzawa, H. Terai, Z. Wang, and R. Shimano, Higgs amplitude mode in the BCS superconductors $Nb_{1-x}Ti_xN$ induced by terahertz pulse excitation, Phys. Rev. Lett. **111,** 057002 (2013).

[16] R. Matsunaga, N. Tsuji, H. Fujita, A. Sugioka, K. Makise, Y. Uzawa, H. Terai, Z. Wang, H. Aoki, and R. Shimano, Light-induced collective pseudospin precession resonating with Higgs mode in a superconductor, Science **345,** 1145 (2014).

[17] N. Tsuji and H. Aoki, Theory of Anderson pseudo spin resonance with Higgs mode in superconductors, Phys. Rev. B **92,** 064508 (2015).

[18] T. Jujo, Quasiclassical theory on third-harmonic generation in conventional superconductors with paramagnetic impurities, J. Phys. Soc. Jpn. **87,** 024704 (2018).

[19] M. Silaev, Nonlinear electromagnetic response and Higgs-mode excitation in BCS superconductors with impurities, Phys. Rev. B **99,** 224511 (2019).

[20] Y. Murotani and R. Shimano, Nonlinear optical response of collective modes in multiband superconductors assisted by nonmagnetic impurities, Phys. Rev. B **99,** 224510 (2019).

[21] N. Tsuji and Y. Nomura, Higgs-mode resonance in third harmonic generation in NbN superconductors: Multiband electron-phonon coupling, impurity scattering, and polarization-angle dependence, Phys. Rev. Res. **2,** 043029 (2020).

[22] G. Seibold, M. Udina, C. Castellani, and L. Benfatto, Third harmonic generation from collective modes in disordered superconductors, Phys. Rev. B **103,** 014512 (2021).

[23] W. V. Budzinski, M. P. Garfunkel, and R. W. Markley, Magnetic field dependence of the surface resistance of pure and impure superconducting aluminum at photon energies near the energy gap, Phys. Rev. B **7,** 1001 (1973).

[24] T. Kubo, Superfluid flow in disordered superconductors with Dynes pair-breaking scattering: Depairing current, kinetic inductance, and superheating field, Phys. Rev. Res. **2,** 033203 (2020).

[25] T. Kubo, Erratum: Superfluid flow in disordered superconductors with Dynes pair-breaking scattering: Depairing current, kinetic inductance, and superheating field [Phys. Rev. Res. 2, 033203 (2020)], Phys. Rev. Res. **6,** 039002 (2024).

[26] S. M. Anlage, H. J. Snortland, and M. R. Beasley, A current controlled variable delay superconducting transmission line, IEEE Trans. Magn. **25,** 1388 (1989).

[27] J. R. Clem and V. G. Kogan, Kinetic impedance and depairing in thin and narrow superconducting films, Phys. Rev. B **86,** 174521 (2012).

[28] N. B. Kopnin, *Theory of Nonequilibrium Superconductivity* (Oxford University Press, Oxford, 2001).

[29] J. Rammer and H. Smith, Quantum field-theoretical methods in transport theory of metals, Rev. Mod. Phys. **58,** 323 (1986).

[30] J. A. Sauls, Theory of disordered superconductors with application to nonlinear current response, Prog. Theor. Exp. Phys. **2022,** 033I03 (2022).

[31] K. Maki, On persistent currents in a superconducting alloy I, Prog. Theor. Phys. **29,** 10 (1963).

[32] K. Maki, in *Superconductivity*, edited by R. D. Parks (Marcel Dekker, Inc., New York, 1969), vol. 2, p. 1035.

[33] M. Yu Kupriyanov and V. F. Lukichev, Temperature dependence of pair-breaking current in superconductors, Fizika Nizkikh Temperatur **6,** 445 (1980).

[34] L. Gor'kov and G. Eliashberg, Generalization of the Ginzburg-Landau equations for non-stationary problems in the case of alloys with paramagnetic impurities, Sov. Phys. JETP **27,** 328 (1968).

[35] G. Eliashberg, Inelastic electron collisions and nonequilibrium stationary states in superconductors, Sov. Phys. JETP **34,** 668 (1972).

[36] S. B. Nam, Theory of electromagnetic properties of superconducting and normal systems. I, Phys. Rev. **156,** 470 (1967).

[37] A. Gurevich and T. Kubo, Surface impedance and optimum surface resistance of a superconductor with an imperfect surface, Phys. Rev. B **96,** 184515 (2017).

[38] T. Kubo, Effects of nonmagnetic impurities and subgap states on the kinetic inductance, complex conductivity, quality factor, and depairing current density, Phys. Rev. Appl. **17**, 014018 (2022).

[39] A. Grankin, V. Galitski, and V. Oganesyan, Negative superfluid density and spatial instabilities in driven superconductors, arXiv:2501.08216.

[40] A. Gurevich, Reduction of dissipative nonlinear conductivity of superconductors by static and microwave magnetic fields, Phys. Rev. Lett. **113**, 087001 (2014).

[41] T. Kubo, Weak-field dissipative conductivity of a dirty superconductor with Dynes subgap states under a dc bias current up to the depairing current density, Phys. Rev. Res. **2**, 013302 (2020).

[42] S. Zhao, S. Withington, D. J. Goldie, and C. N. Thomas, Suppressed-gap millimetre wave kinetic inductance detectors using DC-bias current, J. Phys. D: Appl. Phys. **53**, 345301 (2020).

[43] K. Wang, R. Boyack, and K. Levin, Higgs amplitude mode in optical conductivity in the presence of a supercurrent: Gauge-invariant formulation with disorder, Phys. Rev. B **111**, 144512 (2025).

[44] K. Enpuku, H. Moritaka, H. Inokuchi, T. Kisu, and M. Takeo, Current-dependent kinetic inductance of superconducting YBaCuO thin films, Jpn. J. Appl. Phys. **34**, L675 (1995).

[45] A. J. Annunziata, D. F. Santavicca, L. Frunzio, G. Catelani, M. J. Rooks, A. Frydman, and D. E. Prober, Tunable superconducting nanoinductors, Nanotechnology **21**, 445202 (2010).

[46] M. R. Vissers, J. Hubmayr, M. Sandberg, S. Chaudhuri, C. Bockstiegel, and J. Gao, Frequency-tunable superconducting resonators via nonlinear kinetic inductance, Appl. Phys. Lett. **107**, 062601 (2015).

[47] S. Frasca, B. Korzh, M. Colangelo, D. Zhu, A. E. Lita, J. P. Allmaras, E. E. Wollman, V. B. Verma, A. E. Dane, E. Ramirez, A. D. Beyer, S. W. Nam, A. G. Kozorezov, M. D. Shaw, and K. K. Berggren, Determining the depairing current in superconducting nanowire single-photon detectors, Phys. Rev. B **100**, 054520 (2019).

[48] J. Makita, C. Sundahl, G. Ciovati, C. B. Eom, and A. Gurevich, Nonlinear Meissner effect in Nb$_3$Sn coplanar resonators, Phys. Rev. Res. **4**, 013156 (2022).

[49] X. Dai, X. Liu, Q. He, Y. Chen, Z. Mai, Z. Shi, W. Guo, Y. Wang, L. F. Wei, M. R. Vissers, and J. Gao, New method for fitting complex resonance curve to study nonlinear superconducting resonators, Supercond. Sci. Technol. **36**, 015003 (2023).

[50] J. Greenfield, C. Bell, F. Faramarzi, C. Kim, R. B. Thakur, A. Wandui, C. Frez, P. Mauskopf, and D. Cunnane, Kinetic inductance and non-linearity of MgB$_2$ films at 4 K, Appl. Phys. Lett. **126**, 022602 (2025).

[51] T. Yamashita, S. Miki, K. Makise, W. Qiu, H. Terai, M. Fujiwara, M. Sasaki, and Z. Wang, Origin of intrinsic dark count in superconducting nanowire single-photon detectors, Appl. Phys. Lett. **99**, 161105 (2011).

[52] L. N. Bulaevskii, Matthias J. Graf, and V. G. Kogan, Vortex-assisted photon counts and their magnetic field dependence in single-photon superconducting detectors, Phys. Rev. B **85**, 014505 (2012).

[53] G. Catelani and J. P. Sethna, Temperature dependence of the superheating field for superconductors in the high-κ London limit, Phys. Rev. B **78**, 224509 (2008).

[54] Superheating field of superconductors within Ginzburg-Landau theory, Phys. Rev. B **83**, 094505 (2011).

[55] F. Pei-Jen Lin and A. Gurevich, Effect of impurities on the superheating field of type-II superconductors, Phys. Rev. B **85**, 054513 (2012).

[56] T. Kubo, Multilayer coating for higher accelerating fields in superconducting radio-frequency cavities: A review of theoretical aspects, Supercond. Sci. Technol. **30**, 023001 (2017).

[57] V. Ngampruetikorn and J. A. Sauls, Effect of inhomogeneous surface disorder on the superheating field of superconducting RF cavities, Phys. Rev. Res. **1**, 012015 (2019).

[58] T. Kubo, Superheating fields of semi-infinite superconductors and layered superconductors in the diffusive limit: Structural optimization based on the microscopic theory, Supercond. Sci. Technol. **34**, 045006 (2021).

[59] T. Kubo, How high a field has been and can be achieved in superconducting bulk niobium cavities: The role of RRR, Jpn. J. Appl. Phys. **64**, 018002 (2025).

[60] D. Y. Vodolazov and F. M. Peeters, Superconducting rectifier based on the asymmetric surface barrier effect, Phys. Rev. B **72**, 172508 (2005).

[61] D. Suri, A. Kamra, T. N. G. Meier, M. Kronseder, W. Belzig, C. H. Back, and C. Strunk, Non-reciprocity of vortex-limited critical current in conventional superconducting micro-bridges, Appl. Phys. Lett. **121**, 102601 (2022).

[62] T. Kubo, Tuning critical field, critical current, and diode effect of narrow thin-film superconductors through engineering inhomogeneous pearl length, Phys. Rev. Appl. **20**, 034033 (2023).

[63] Y. Hou, F. Nichele, H. Chi, A. Lodesani, Y. Wu, M. F. Ritter, D. Z. Haxell, M. Davydova, S. Ilic *et al.*, Ubiquitous superconducting diode effect in superconductor thin films, Phys. Rev. Lett. **131**, 027001 (2023).

[64] T. Kubo, Numerical data underlying the figures in "Higgs-mode-induced instability and kinetic inductance in strongly dc-biased dirty-limit superconductors", Zenodo (2025), https://doi.org/10.5281/zenodo.15377256.